Kaunas University of Technology

Faculty of Mechanical Engineering and Design

Development of an Advanced Ultrasonic Method for Inspection of Aircraft Main Landing Gear Tie-Bolts

Master's Final Degree Project

Laurynas Duoba

Project author

Prof. Dr. Elena Jasiūnienė

Supervisor

Kaunas, 2021

Kaunas University of Technology

Faculty of Mechanical Engineering and Design

Development of an Advanced Ultrasonic Method for Inspection of Aircraft Main Landing Gear Tie-Bolts

Masters's Final Degree Project

Aeronautical Engineering (6211EX024)

Laurynas Duoba

Project author

Prof. Dr. Elena Jasiūnienė

Supervisor

Assoc. Prof. Saulius Japertas

Reviewer

Kaunas, 2021

Kaunas University of Technology

Faculty of Mechanical Engineering and Design

Laurynas Duoba

Development of an Advanced Ultrasonic Method for Inspection of Aircraft Main Landing Gear Tie-Bolts

Declaration of Academic Integrity

I confirm the following:

1. I have prepared the final degree project independently and honestly without any violations of the copyrights or other rights of others, following the provisions of the Law on Copyrights and Related Rights of the Republic of Lithuania, the Regulations on the Management and Transfer of Intellectual Property of Kaunas University of Technology (hereinafter – University) and the ethical requirements stipulated by the Code of Academic Ethics of the University;

2. All the data and research results provided in the final degree project are correct and obtained legally; none of the parts of this project are plagiarised from any printed or electronic sources; all the quotations and references provided in the text of the final degree project are indicated in the list of references;

3. I have not paid anyone any monetary funds for the final degree project or the parts thereof unless required by the law;

4. I understand that in the case of any discovery of the fact of dishonesty or violation of any rights of others, the academic penalties will be imposed on me under the procedure applied at the University; I will be expelled from the University and my final degree project can be submitted to the Office of the Ombudsperson for Academic Ethics and Procedures in the examination of a possible violation of academic ethics.

Laurynas Duoba
Confirmed electronically

Kaunas University of Technology

Faculty of Mechanical Engineering and Design

Study programme: Aeronautical Engineering (6211EX024)

Task of the Master's Final Degree Project

Given to the student: Laurynas Duoba

1. Title of the Project:

Development of an Advanced Ultrasonic Method for Inspection of Aircraft Main Landing Gear Tie-Bolts

Pažangaus ultragarso metodo, skirto tikrinti orlaivio pagrindinės važiuoklės tvirtinimo varžtus, sukūrimas

2. Aim of the Project:

To develop advanced ultrasonic method for inspection of main landing gear tie-bolts.

3. Tasks of the Project:

1. To perform the literature analysis of NDT techniques, which are used or could be used for inspection of tie-bolts and to perform analysis of root cause of large number tie-bolts.
2. To design the computerized model of tie-bolt in CIVA NDT software and perform ultrasound immersion method analysis.
3. Perform parametric and computation studies using CIVA NDT software of detectability of the defects depending on the size, position and angle using currently used ultrasonic techniques.
4. To develop advanced phased array method for tie-bolt defects detection.
5. Comparison of currently used ultrasonic inspection method with the advanced phased array method for tie-bolt defects detection.

4. Structure of the Text Part:

Introduction, literature review, computer model of the tie-bolt inspection, computation analysis, phased array development.

5. Consultants of the Project:

Author of the Final Degree Project	Laurynas Duoba	2020-02-04
	(name, surname, date)	
Supervisor of the Final Degree Project	Prof. Dr. Elena Jasiūnienė	2020-02-04

(abbreviation of the position, name, surname, date)

Head of Study Programmes Prof. Artūras Keršys 2020-02-04

(abbreviation of the position, name, surname, date)

Duoba Laurynas. Development of an Advanced Ultrasonic Method for Inspection of Aircraft Main Landing Gear Tie-Bolts. Master's Final Degree Project / supervisor prof. dr. Elena Jasiūnienė; Faculty of Mechanical Engineering and Design, Kaunas University of Technology.

Study field and area (study field group): Aeronautical Engineering (E14), Engineering Science.

Keywords: ATR42, tie-bolt, ultrasound, matrix phased array.

Kaunas, 2021. 66 pages.

Summary

The purpose of this work is to develop advanced ultrasound method for aircraft main landing gear tie-bolt inspection. To carry out the research it is necessary to perform further tasks: review information sources on currently used NDT methods, create computerized main landing gear tie-bolt model, test the theoretical model using CIVA NDT software, develop more advanced ultrasound method and determine more reliable method.

Main landing gear wheel halves are connected with tie-bolts, where on ATR42 aircraft, there are 10 bolts per wheel installed. Each bolt is tested with dye penetrant, magnetic particle, eddy current or ultrasound NDT methods every wheel overhaul cycle. One of the problems with currently used inspection methods are increased tie-bolt failure rate in service. Theoretical possibilities to inspect tie-bolt with matrix phased array method was performed and compared to currently used ultrasound immersion pulse-echo method, it was determined that matrix phased array is more suitable choice for inspection of defects. Theoretical analysis was performed, and results obtained.

Duoba Laurynas. Pažangaus ultragarso metodo, skirto tikrinti orlaivio pagrindinės važiuoklės tvirtinimo varžtus, sukūrimas. Magistro baigiamasis projektas. Vadovė prof. dr. Elena Jasiūnienė; Kauno technologijos universitetas, Mechanikos inžinerijos ir dizaino fakultetas.

Studijų kryptis ir sritis (studijų krypčių grupė): Aeronautikos inžinerija (E14), Inžinerijos mokslai.

Reikšminiai žodžiai: ATR42, jungiamasis varžtas, ultragarsas, matricinė fazuota ultragarsinė gardelė.

Kaunas, 2021. 66 p.

Santrauka

Šio darbo tikslas yra sukurti pažangesnį ultragarso metodą, skirta orlaivio pagrindinės važiuoklės tvirtinimo varžtų patikrinimui. Tyrimui atlikti, būtina atlikti šias užduotis: peržiūrėti informacijos šaltinius apie šiuo metu naudojamas neardomosios kontrolės tikrinimo metodus, sukurti kompiuterinį pagrindinės važiuoklės tvirtinimo varžto modelį, išbandyti teoretinį modelį naudojant CIVA NDT programinę įrangą, sukurti tobulesnį ultragarso metodą ir nustatyti patikimesnį metodą.

Pagrindinės lėktuvo ATR42 važiuoklės rato pusės yra sujungtos varžtais, kur viename rate yra 10 jungiamųjų varžtų. Kiekvienas varžtas yra tikrinamas dažų prasiskverbimo, magnetinių dalelių, ultragarso neardomosios kontrolės metodais, kiekvieną rato remonto ciklą. Vieną iš šiuo metu naudojamų tikrinimo metodų problemų yra padidėjęs varžtų trūkimų kiekis, lėktuvo serviso metu. Buvo atliktos teorinės galimybės patikrinti tvirtinimo varžtą matricinės fazuotos gardelės metodu ir palyginta su šiuo metu naudojamu ultragarso metodu. Buvo nustatyta, kad matricinės fazuotos gardelės metodas yra tinkamesnis varžto defektam aptikti. Buvo atlikta teorinė analizė ir aprašyti rezultatai.

Table of Contents

List of Figure

List of Tables

Introduction

Main landing gear tie-bolts are being used on all aircraft types and are considered extremely safety-critical components since they hold two halves of the wheel together. Landing gear wheel bolts must be able to withstand high loads during landings. Together with landings, often tightening of the bolts can result in cracks due to bolt stretching. Usually, the bolts are inspected by dye penetrant or magnetic particle methods for every unscheduled wheel repair. There are ten bolts installed per wheel on ATR 42-300/500 aircraft, and there are four main landing gear wheels in total. The latest investigation has revealed that during 2018, DAT LT has replaced 33.7 % and during 2019, 42% of bolts inspected, as well recorded growth in broken bolts reported in service. In case broken wheel bolt in-service aircraft is considered unserviceable before wheel replacement. Additional non-destructive inspections, more often wheel replacements, wheel repairs, and aircraft unserviceability, can expose the company to increased costs. Finding more precise non-destructive testing methods or other means of changes in procedures would reduce additional expenses related to wheel maintenance.
This thesis was motivated by the need to detect cracks reliability in the tie-bolts of the landing gear, as recently, the increase in the broken tie-bolts of ATR 42-300/500 main landing gear was observed.

Project aim – To develop advanced ultrasonic method for inspection of main landing gear tie-bolts.

Project tasks:

1. To perform the literature analysis of NDT techniques, which are used or could be used for inspection of tie-bolts and to perform analysis of root cause of the large number of tie-bolts.
2. Design the computerized model of tie-bolt in CIVA NDT software and perform ultrasound immersion method analysis.
3. Perform parametric and computation studies using CIVA NDT software of detectability of the defects depending on the size, position and angle, using currently used ultrasonic techniques.
4. To develop advanced phased array method for tie-bolt defects detection.
5. Comparison of currently used ultrasonic inspection method with the advanced phased array method for tie-bolt defects detection.

1. Literature analysis

Between 2018 and 2020, DAT Airlines witnessed a number of broken/shared tie bolts on ATR 42 main wheels. Tie bolts are being inspected by dye penetrant or magnetic particle inspection every tire change. In case any cracks are observed, tie bolts near the crack detected bolt must be inspected as well. It was noted that fatigue cracks on these bolts are typically „closed cracks", making it challenging to get dye penetrant inspection into the crack. It's also challenging to get bolts clean enough to use dye penetrant since dust, dirt, and lubricant can block any open cracks, thus preventing dye penetrant from getting into the crack.
To check if dye penetrant or magnetic particle inspection is sufficient to detect early cracks, different bolts from in-service aircraft will be analyzed to determine the most suitable inspection method to prevent broken bolts and early cracks detection.

1.1. Effect diagram

To investigate the root cause of the large number of broken tie bolts, a fishbone diagram developed by Kaoru Ishikawa was constructed. The diagram looks like fish skeleton, where the head is the problem and the causes for the problem is feeding into the spine. The fishbone diagram could be referred to as a thinking process to investigate the event's root cause. Fishbone diagram for ATR 42-300 main landing gear wheel tie-bolt failure is shown in figure 1.1.
[1]

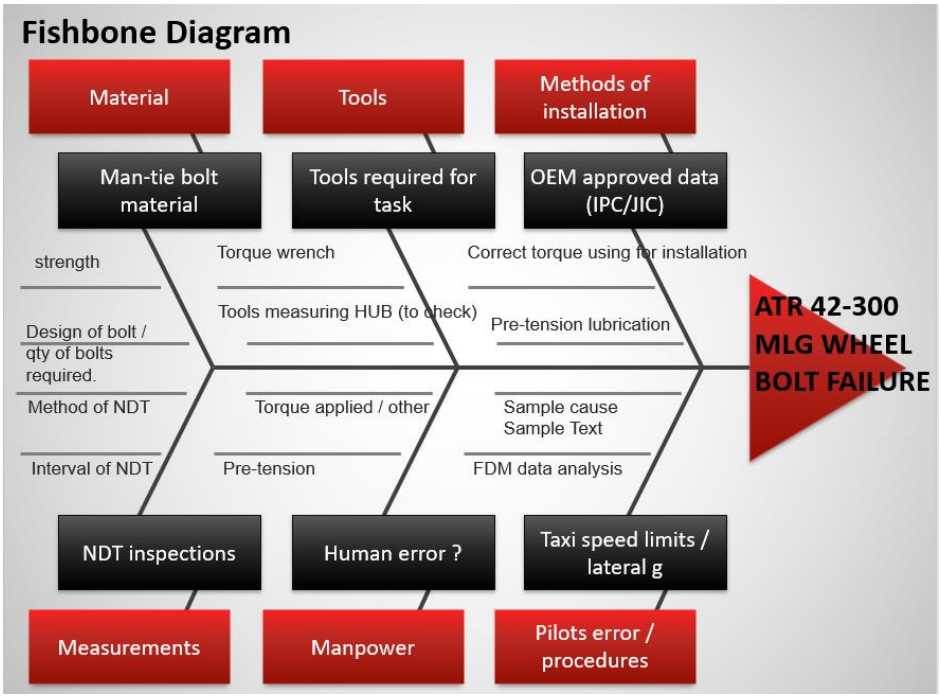

Figure 1-1. Fishbone diagram

The factors identified in the diagram may not be significant; however, they allow them to be identified and sorted out systematically. In other words, it is better to identify all possible failure reasons and then eliminate least likely. As soon as the diagram is complete, all branches could be traced back to identify major causes and eliminate minor ones. [1]

1.2. Material

Wheels and tires are one of the most highly stressed parts in aviation. Due to impact loads, cyclic loads, burnouts, or corrosion, it can fail. In case of a failure event, it could result in an excellent safety thread. During manufacturing tests and as per FAA standard (TSO -C26c), the wheels must withstand radial loads, axial loads, and a combination of both. During the test, the wheel needs to roll a predefined distance under a specific load, and after the test, no cracks could be detected. [2]
As per described cause-effect diagram, tie-bolt design is suspected as one of the root causes of main landing gear wheel failure. During 2018-2019 DAT has identified a high failure rate of wheels tie-bolts inspected in the shop. During 2018, the finding rate was 33.7%, and during 2019 – 42%. The majority of the inspections resulted in cracks or corrosion detected.

1.3. Fatigue failure in bolts

Fatigue damage is often used to describe the damage to a component that has been sustained because of loading. During these days, it could be equated to crack length. In critical usage of bolts, periodical inspections are required as dye penetrant or even x-rays to ensure that there are no cracks. Fatigue in bolts is very rare since fatigue cracks propagate because of a changing tensile strength, and nuts are under compressive stress, so any pre-existing cracks are not propagating.[3] [4]
Since fatigue is a progressive cracking, it could start at some existing defect, such as inclusion in the metal and slowly growing in length during each loading. It could require numerous stress cycles before the crack could be visible. While crack is increasing, the material receives higher stress since there is less area to hold the loading. After critical length is reached, a crack will progress all the way through the material resulting in complete failure. [3]

1.4. Main landing gear wheel failure

During 2017 during a Boeing 737 taxi, the crew heard a loud noise as what they thought was a tire burst on the left landing gear; however, after engineer evaluation, the left-hand outboard wheel had failed as shown in figure 1.2. During the Australian Transport Safety Bureau investigation, it was found that one main wheel ruptured due to tie bolt assemblies that had loosened while in service, which allowed two-wheel halves to move relative to each other, resulting in a fatigue crack and eventually wheel rupture.

Figure 1-2. Damage to the number one main wheel assembly on VUH [5]

Manufacturers performed further detailed analysis and concluded that the wheel failed because of founding fatigue cracks. A small crack was also noticed in the tie bolt hole; however, it did not appear to be the main root cause. The manufacturer visited the airline's repair shops to confirm that wheel repair procedures were appropriate. 2 out of 3 repair shops were found to be working entirely in compliance with manufacturer requirements. During the visit to one repair station, it was found silicon grease on the wheel halves' mating faces. However, this shop has not performed any repairs on the wheel mentioned in the report. [5]

Another failure of wheel assembly happened to corporate passenger jet. The mentioned wheel had no interval for bolts lifetime, only periodical inspections as per manufacturer maintenance program. It was described that bolts on this aircraft remain in service for 4000-5000 cycles, and nuts are changed around 400 cycles.

Twelve bolts of failed wheels were photographed after visual inspection with a light microscope as shown in figure 1.3. Four bolts were found bent, four bolts exhibited stripped threads near bolt ends, and four bolts had no damage as per visual inspection.

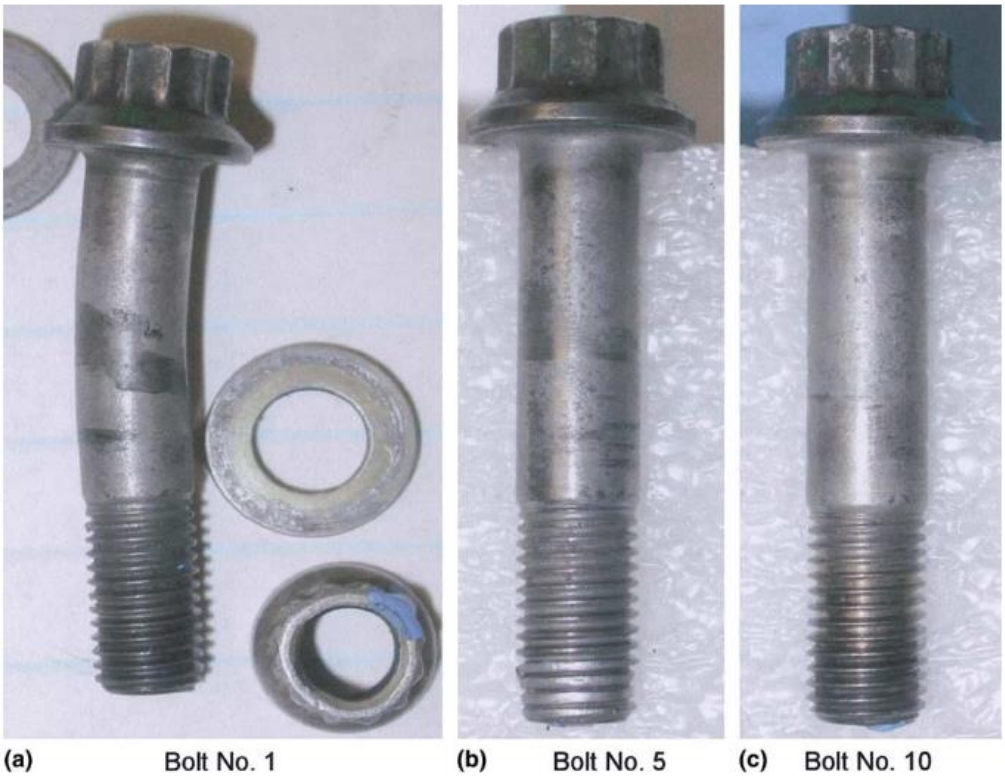

Figure 1-3. Photographs of bolts from each damage category: (a) bent; (b) stripped (note last four threads of Bolt #5), and (c) no apparent damage [6]

Bolt thread profiles were examined by an optical compensator, producing a profile every 15 degrees around the circumference. On bolt numbers 9,11, and 12, there were no remarks observed. Bolt 10 exhibited steps on the load-bearing daces of certain threads, which occurred on only seven threads as shown in figure 1.4. Mentioned stepped threads are located under the nut when it's in the tightened position. Bolts 1-8 was examined as well, and number 3-8 had stripped threads; however, steps were not like steps found in bolt number 10.

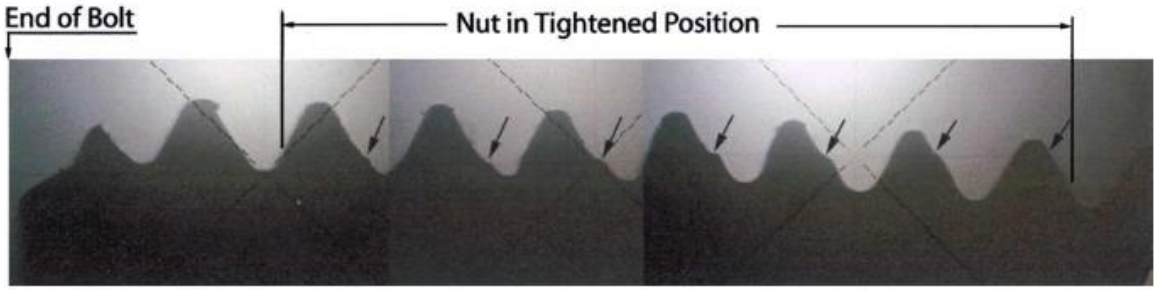

Figure 1-4. Optical compensator image of threads of Bolt #10, showing the steps on thread faces [6]

Mentioned steps were a result of overload transmitted by the nut. The steps were produced while the nut was in tightened position, and since steps appear to be on one side, it indicates that the load on the one side was relieved and overloaded on the other side, causing deformation. Moment caused by difference in the load lines could be seen at figure 1.5.

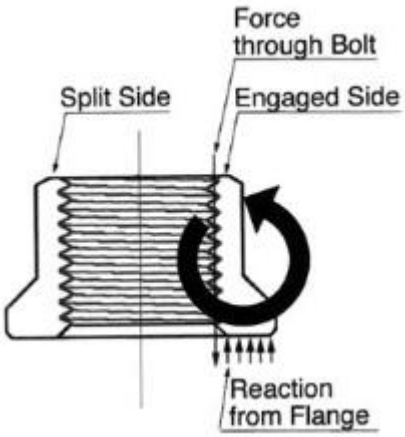

Figure 1-5. Moment caused by the difference in the load lines [6]

It was concluded that the root cause of the wheel failure was a cracked nut. After the nut cracked, loads on the tie-bolt were released. Increased load moved to further bolts/nuts couples, which, due to increased load backed off, and so on around all circles. The suspected root cause of the cracked nut was hydrogen embrittlement. Crack initiation could have resulted in service loads or tightening. [6]

1.5. Fatigue testing

According to the American Society of Metals – Metals Handbook 1975 & 2008, between 80% to 90% of all mechanical service failures can be attributed to fatigue. It is critical to test the fatigue properties during experiments to understand failure occurrences.
Fatigue failures will happen when a material is loaded repeatedly with a lower stress level than a level, which would cause immediate failure. With each cycle, material damage will progress.
The fundamental purpose of fatigue tests is to understand the stress level safely used within the described interval. More complex fatigue tests could produce better insight into how fatigue damage evolves and shows how a specific component's performance will change during its service life. [7]

1.6. Experimental testing

In 2020, the University of Sidney has performed an experiment and analysis of fatigue behaviour of stainless-steel bolts in tension and shear under constant-amplitude loading. [8] These experimental and research parts explain how tie-bolt could be analyzed in DAT case if the equipment would be available.
To achieve results, static and cyclic testing were performed, where 250 kN fatigue testing machines were used, as shown in figure 1.6 During this experiment tightening effect was not considered. During static tension tests, ultimate strength and load-deformation relationships were received. Load speed was 0.5 mm/min, and displacements were monitored by photoelectric sensors. For fatigue test, periodic load with constant amplitude were performed. [8]

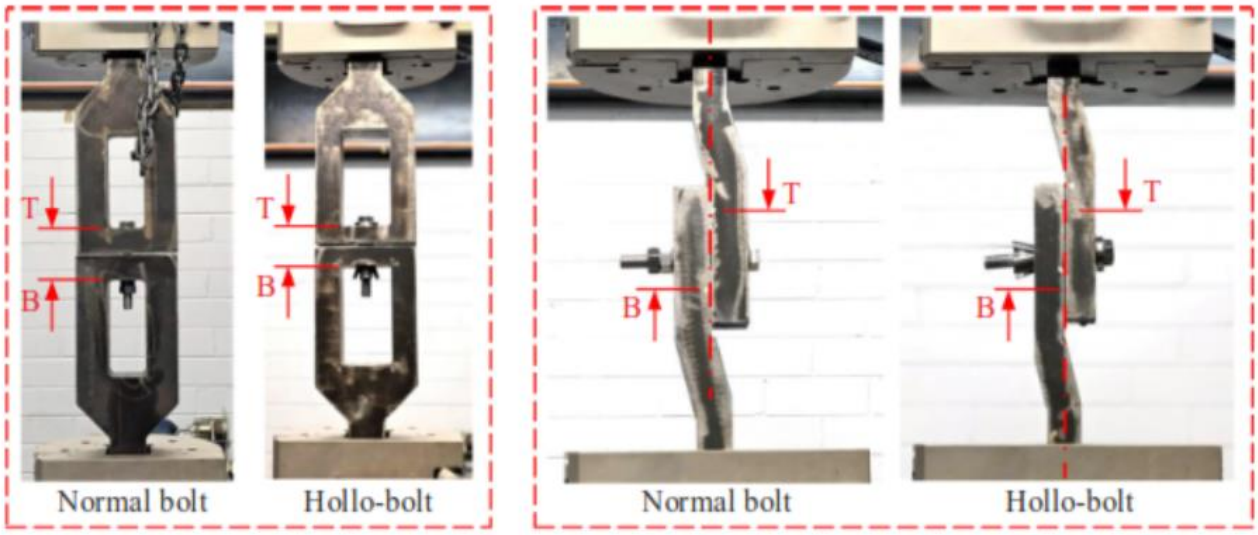

Figure 1-6. Test setup [8]

Static results for static tension of normal bolts, static shear of normal bolts, and fatigue tension of normal bolts, fatigue shear of normal bolts were received, the further relationship between stress ranges and failure cycles were collected and presented as shown in figure 1.7.

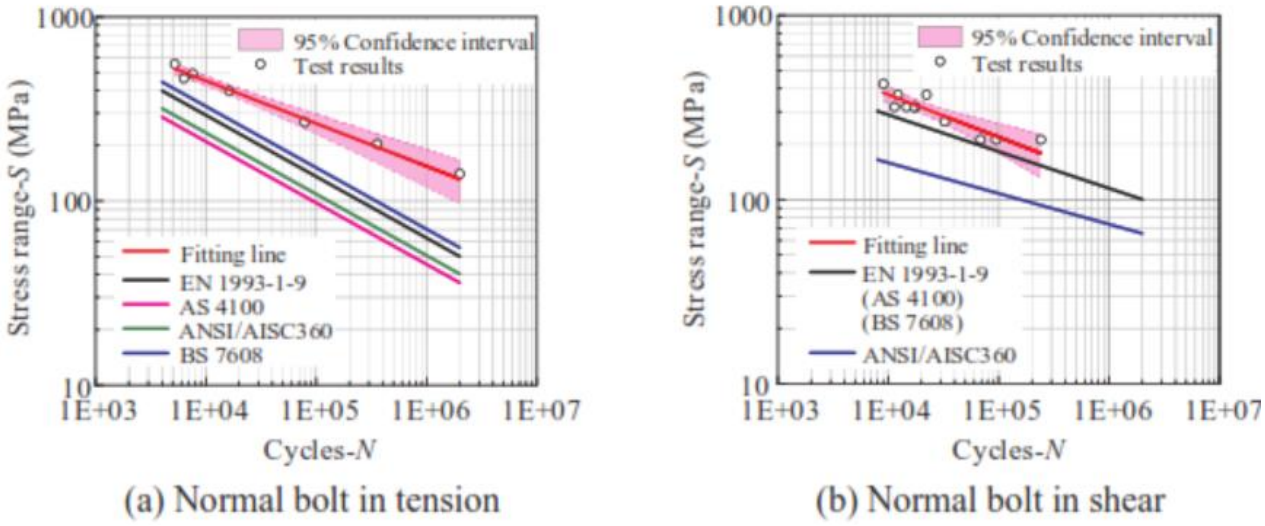

Figure 1-7. S-N curves of stainless steel bolts and comparison with design codes [8]

To show stress progress through the loading finite element method was adopted. Three-dimensional models were created and analyzed using Abaqus software, as shown in figure 1.8.

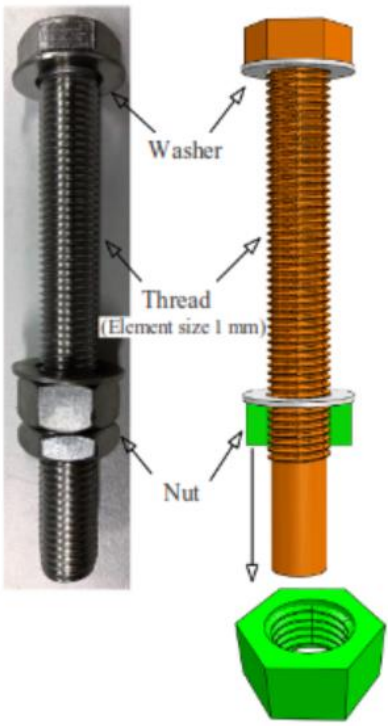

Figure 1-8. Components in numerical models [8]

1.7. Tools and Methods of installation

ATR aircraft wheels are being inspected every line check, which is every three calendar days, not exceeding 72 hours. Inspection as a requirement is stated in the ATR maintenance planning document and must be performed in accordance with manufacturer maintenance procedures.[9]
During the inspection, visual inspection is being performed, tire pressures checked, leak tests of the inflation valve assembly are performed. Conditions of tire wear limit are described as cuts, cracks, bulges, indentations, thread separation, chunking, etc. In case any of the findings, which are out of limits, observer tire/wheels replacement might be necessary.
Strict installation procedures must be followed, especially pre torque, final torque, which is given in aircraft maintenance manuals and depends on wheels part numbers. Incorrect torque selected could lead to too much or too little preload. [10]

1.8. Preload

Preload has a direct impact on ATR wheels bolt safety and reliability during installation. If there will be too much preload, plastic deformation of the bolt or short-term failure of the bolt could occur. Preload level results from tightening torque given in maintenance manual, and it represents parameter showing stresses distributions under actual loading conditions. If there will be too little preload, it will lead to accelerated fatigue cracking of the fastener.
University of Naples Federico II has simulated shear behavior on the bolt under tensile and preload conditions as shown in figure 1.9.

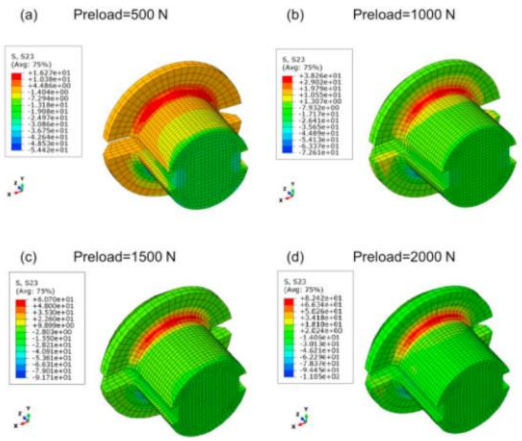

Figure 1-9. Shear stress distribution in MPa on the bolt under applied tensile load F=1000 N by varying the bolt preload [11]

It could be noticed that, shear stress on the bolt section to the plates decrease as the preload increase. Tensile load transferred to the bolt decreased linearly as preload increased. [11]
Proper preload during bolt installation will help to resist external loading and keeps the join interface in compression. Improper preload is one of the human errors, which can lead to catastrophic events. [12]

1.9. Flight Data Monitoring

Introduction to FDM:

Flight data monitoring is a very useful tool for every operator, which helps to improve and monitor operational safety. For commercial aircraft, which operate under European territory, flight data monitoring is mandated.
Flight data monitoring (FDM) is a program used for collecting and analyzing data recorded during routine flights. Analyzed data support crew performance, operational procedures, flight training. [13], [14]

Data recovery, processing, and analysis:

During DAT case, investigation on ATR 42/72 family aircraft performed. To recover data, the most suitable option for this type of aircraft is to get the MPC's PCMCIA card. Each type of card is removed from an aircraft, and another card must be inserted. The standard rate of card removal is set on a weekly basis; however, it depends on card capacity and internal operator procedures. Wireless data transfer solutions exist already, however in DAT case, mentioned modification is not applicable.

In DAT case, data is processed by Aerobytes software. It provides a series of flights and flight events to the end-user. The quality of the database could be assessed by retrieval rate and the quality index. Retrieval rate is the ratio of the number of flights processed by the FDM software comparing to the actual number of flights performed.

Flight data monitoring:

As per the presented fishbone diagram, one of DAT LT suspected reasons of main landing gear tie-bolt failure was limited on max G force during a turn while taxing on the ground (lateral g). The comments were requested from the original equipment manufacturer.
After ATR has performed an investigation with a dedicated design office, it was reported that the landing gears had been designed to sustain a lateral load factor of 0.5G regarding a steady turn. This value (0.5G) does not consider a braking action that should be entailed by the pilot. Therefore, a lateral load factor of 0.3G can be considered as relevant, considering data monitoring during on ground.

FDM analysis:

For further analysis, it was selected to investigate DAT LT ATR 42-300 and ATR 42-500 flights since 2019.01.01 until 2020.10.10.
Using software "Aerobytes", 10 453 flights since 01 January 2019 were analyzed. The lateral G values on the ground oscillate between 0.07 – 0.13G, which is not even close to ATR suggested limits. Looking historically, the highest recorded value was in the region of 0.2-0.25 G, which does not reach the ATR proposed minimal value of 0.3G for monitoring events. Longitudinal G values (accelerating or braking) recorded over many flights are as follows: light braking 0.15-0.2G, normal braking 0.2-0.25, heavier than normal up to 0.3G, and heavy braking >0.3G. Most take-off accelerations are in the 0.1-0.15G range. In other words, lateral G on ground values of 0.1-0.2G is consistent with other comparable G values.
It was recorded and agreed that DAT case, lateral G was not the reason for tie-bolt fracture; however, Flight Data Monitoring values were changed to:
Red: > 0.3
Yellow: > 0.2
Green: > 0.15

1.10. NDT technologies

Non-destructive testing (NDT) techniques have a significant impact on aviation reliability and safety monitoring due to cost savings and efficiency. Non-destructive testing (NDT) is a particular technique for detecting, locating, recognizing, and measuring the internal structure of material or component without causing damage for effectiveness or reliability. The most commonly used NDT techniques are: Ultrasonic, X-rays, magnetic particle, penetrant testing, eddy current, and so on. [15] [16]

1.11. Dye penetrant inspection

Dye penetrant inspection is one of the oldest NDT methods; however, due to the small amount of time needed and low costs, it is one of the methods used in aviation frequently. This method helps to detect cracks, incomplete fusion, fractures, grinding, etc. Same as magnetic testing, ultrasound or eddy current, dye penetrant is classified as contact method. [17]

The principle of dye penetrant is where low surface tension fluid penetrates the dry and clean surface. Most often, penetrants are applied by spraying or brushing; after some time, the penetrant is removed, and the developer is applied, which draws the penetrant out, further invisible indication becomes visible as shown in figure 1.10. During the inspection, ultraviolet or white light are used. The type of light depends on the type of dye. [18]

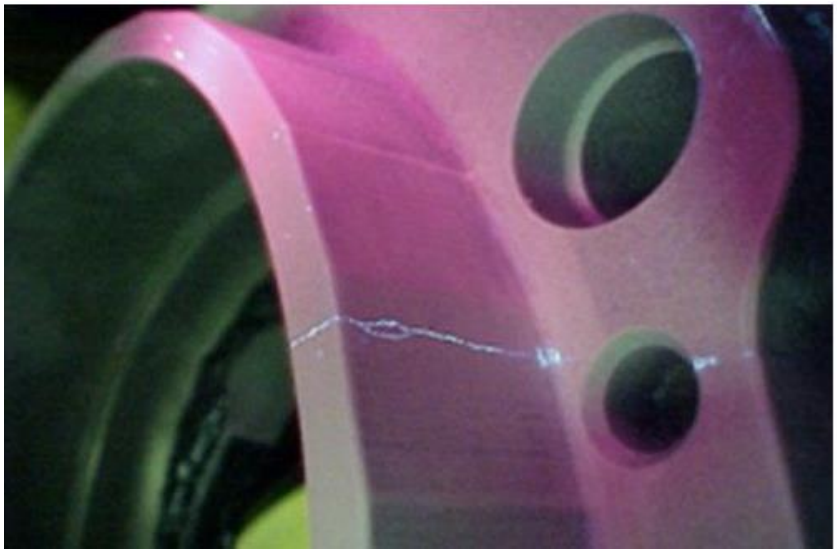

Figure 1-10. Dye penetrant method used on the wheel assembly [18]

Advantages of dye penetrant method usage on wheel bolts:
- Fluorescence ensures good visibility for cracks.
- Time and cost-effective method.
- Simple to train staff to use method.

Disadvantages:
- Cracks inside bolts cannot be observed.

1.12. Dye penetrant procedure – crack inspection

Dye penetrant inspection could be used to find cracks in all ferromagnetic wheel and brake components that must have an inspection for crack. The vendor provides information regarding fluorescent penetrant fluids.
Before the inspection, components must be cleaned as much as possible, and paints must be removed if applicable. Inspection should follow fluorescent penetrant processing specifications, such as ASTM 1417. Penetrant materials must be in compliance with SAE AMS 2644, type 1, sensitivity level 2.
During the analysis of a crack indication, the decision whether the indication is false, not important, or important should be made. False indications could be caused by poor removal of developers or too much developer. Not important indications could be caused by discontinuities in component design. Important indications mean actual discontinuities found during an inspection.
Fatigue cracks are considered important indications and must be removed from service; however, it would be recommended to perform another NDT method to confirm fatigue crack. If the component

maintenance manual allows, it is possible to perform repairs. After the repair is performed, dye penetrant inspection should be performed to ensure that fatigue cracks no longer exist. [19]

1.13. Magnetic particle inspection

As dye penetrant, magnetic particle method is very simple and widely used due to time and costs benefits, as well it is highly portable. Usually, during this method, cracks are being evaluated manually, however automated technologies based on machine vision has recently been analyzed. [20] During magnetic particle inspection method, while magnetic current runs through the component, any defect as a crack in the material will interrupt the current flow and will cause magnetism as shown in figure 1.11. This will cause a flux leakage field at the damaged area. [21]
Although this method is being frequently used in aviation, it has some limits. To use magnetic particle inspection, the material of the component must be ferromagnetic. Also, MPI inspection only detects effects, which are near to the surface.

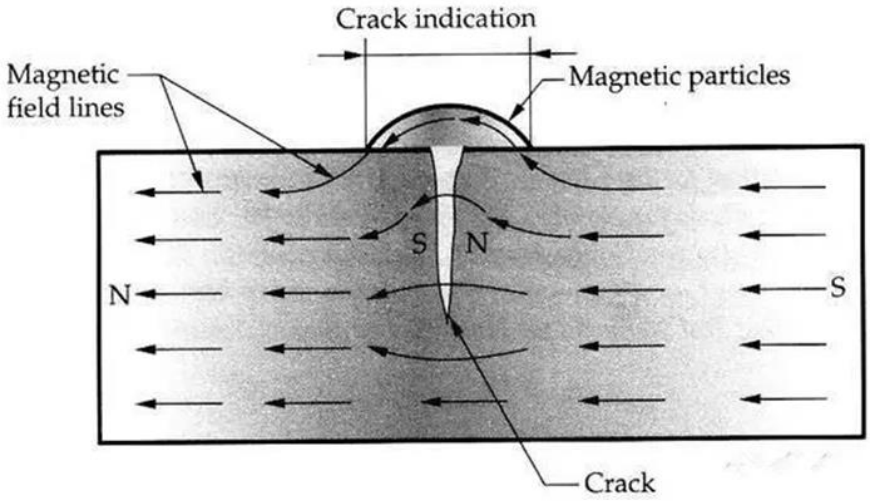

Figure 1-11. Schematic of magnetic particle inspection [21]

Advantages of dye magnetic particle usage on wheel bolts:
- Shows surface and near-surface defects.
- Pre-cleaning is not needed.

Disadvantages:
- Messy method.
- Internal defects could not be detected.

1.14. Magnetic particle inspection procedure

A magnetic particle inspection is being done to find cracks in all ferromagnetic bolts. Magnetic field should find crack on a surface in all areas. Specification ASTM-E1444, standard practice, or similar manual should provide magnetizing values for part inspection. Wet magnetic particles should strictly follow the standards given in specification ASTM-E1444.

During equipment adjustment, the component should be placed in the magnetic field, which should pass through the surface of the part in two directions vertical to each other. Fatigue cracks should be inspected while using a wet continuous method of magnetic particle examination. Magnetizing values should be set from specifications ASTM-E1444.
During the inspection, all parts must be carefully inspected where fatigue is likely to be the root cause of failure. For bolts, special attention is needed to the radius between the bolt head and bolt shank. Also, the area near the third and fourth thread from the shank should be inspected. Further full wave rectified alternating current should be used, or half-wave rectified alternating current or an alternating current in the magnetic power source should be used. Where possible, longitudinal magnetization after circumferential magnetizations must be performed. Demagnetization is required if the magnetizing force used for magnetization is less than the magnetization force used for a preceding magnetization.
Crack orientation is usually vertical to stress direction. However, crack indications could happen where there are sudden thickness of section change, parts are pressed, or welded areas. If possible, it is recommended that noticed cracks would be inspected by eddy current inspection in order not to reject components due to false crack indication.
If any cracks are detected, they must be removed from service; however, before, it is necessary to check if the component maintenance manual allows repair. If a part was repaired, magnetic particle inspection should be performed once again to ensure that fatigue cracks were eliminated. [22]

1.15. Eddy current method

The eddy current technique involves the use of a coil, which carries an alternating current near the testing unit. After eddy currents hit specimen, as shown in figure 1.12.

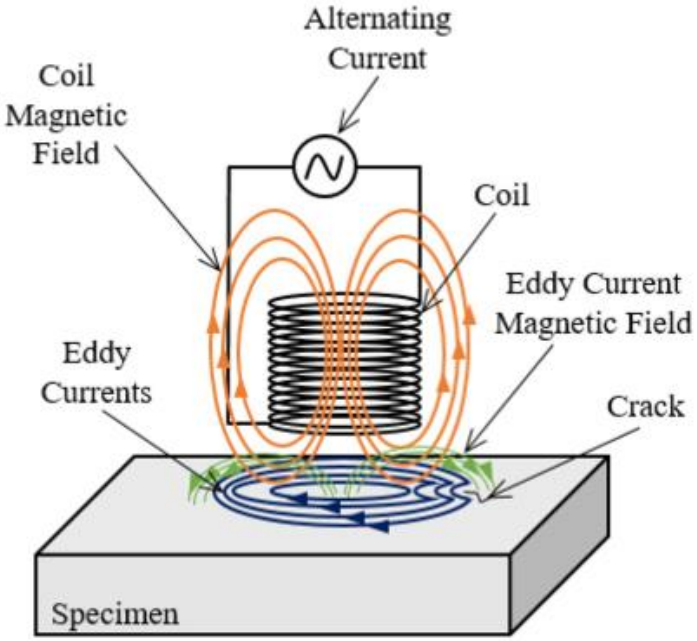

Figure 1-12. Eddy current method schematic [23]

The magnetic flux is measured, and changes in it will indicate the changes within the material, for example – cracks. Eddy's current technique is very sensitive and can detect a crack, the minimum length of which is 25 μm.
Eddy current is a frequently used method in the aviation sector. Due to sensitivity, it is mainly used in structures and subsurface inspections, bolt hole inspections, conductivity measurements, etc. However, it is worth mentioning that the eddy current needs direct access to the damage, and it must have contact, which makes difficulties with already contacting surfaces. [23] [24]

1.16. Eddy current inspection procedure

Eddy current inspection could be performed while using different instruments, which will hold its own procedures; however, the non-destructive testing manual recommends using equipment, which is able to find reference standards given when test frequencies in the range of 100 kHz to 500 kHz are used.
Before proceeding with eddy current inspection on wheel or subassemblies, loose paint, tire rubber, and other unwanted materials from subassembly shall be removed. Test equipment should be switched on and connected to the appropriate test coil as per manufacturer requirements. After test coil scanning over reference notch, adjustment of an instrument is needed to get a minimum signal of 40% of the full-scale height.

1.17. Eddy current in bolts structure health monitoring

Periods in bolt cracking could be described as crack initiation, crack propagation, and rapid fracture. If crack propagation exists, a warning could be notified before the rapid fracture period. In the majority of bolts fracture cases, it could be noticed that warning before the rapid fracture period was not observed, even with periodic NDT inspections. In 2020, Xiamen University verified one of the possible structural health monitoring solutions to monitor the structural performance of bolted joints in real-time.
The solution is based on two configurations of the sensing film, where one of them is a one-dimensional coil array, and another is a two-dimensional coil array, both having the ability to identify crack parameters, such as crack angle, depth, and crack location in the axial bolt direction. The concept is shown in figure 1.13.

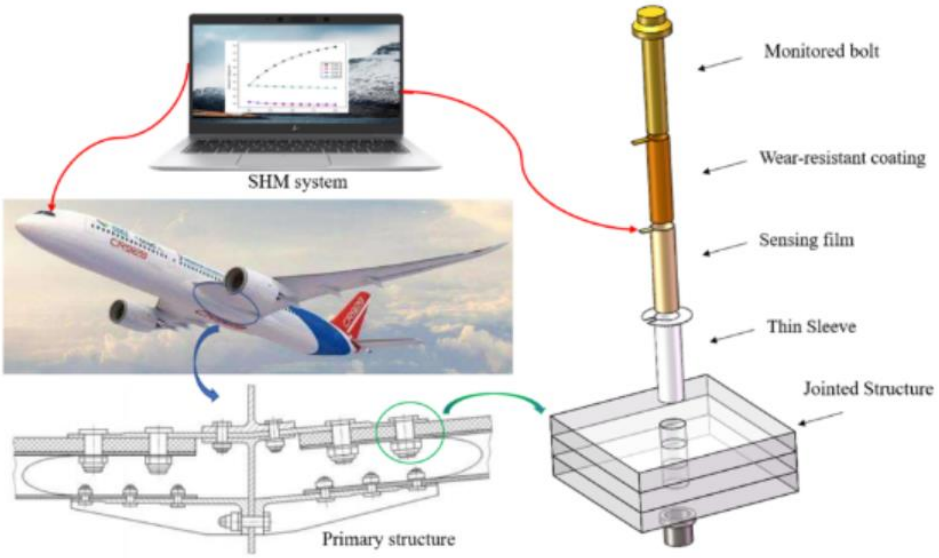

Figure 1-13. The structure health monitoring (SHM) system for monitoring the process of the bolt cracking [25]

While using this method, the crack depth could be determined in the range of 100 kHz to 1 Mhz. [25]

1.18. Ultrasound method

The principle of the pulse-echo method is shown in figure 1.14, where the generated ultrasonic wave is reflected by the back wall of testing material and obtained by received. Further, a signal is displayed on the screen.

To measure the velocity of ultrasound waves, there are need to determine the distance the wave travels and the time, which takes to pass through it. If measurements are being done by the pulse-echo method, the wave will travel distance, which is two times more than material thickness. The velocity of the wave could be determined by dividing two times thickness of the sample by the signal time of flight. [26]

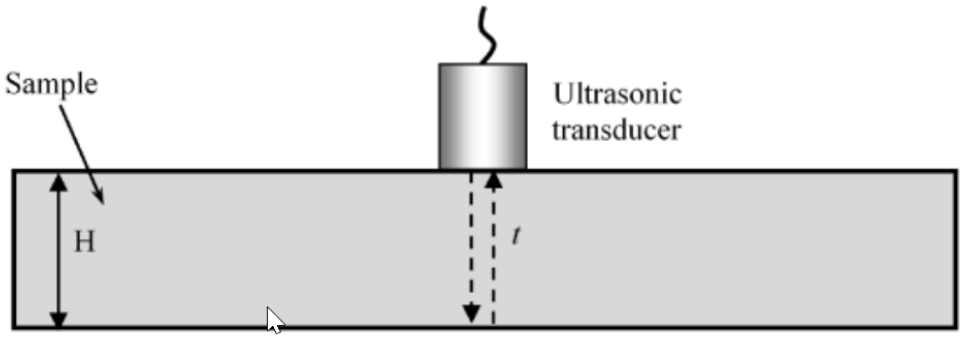

Figure 1-14. Ultrasonic velocity measurement by using pulse-echo method [27]

If the pulse-echo method are applied, display will indicate the initial pulse, and after some time, the pulse reflected from the back wall could be noticed, as shown in figure 1.15. [27]

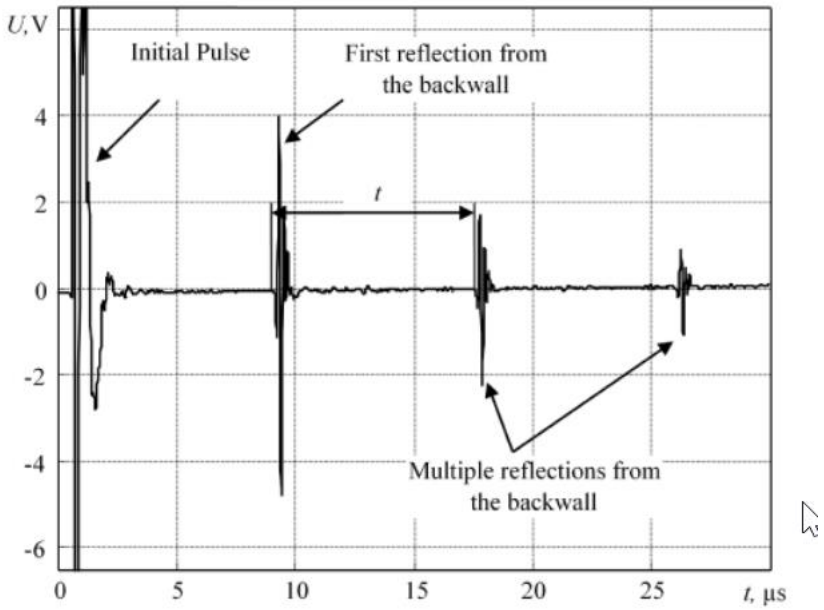

Figure 1-15. Example of the signal in the time domain [27]

During ultrasound tests, we can evaluate crack path and shape by using a technique to produces images from ultrasound wave response. This could be achieved through an array of ultrasound transducer elements, which are known as ultrasound transducer arrays. The crack total focusing method is used (TFM) together with phase coherence imaging (PCI) to determine crack tip location and length as shown in figure 1.16.

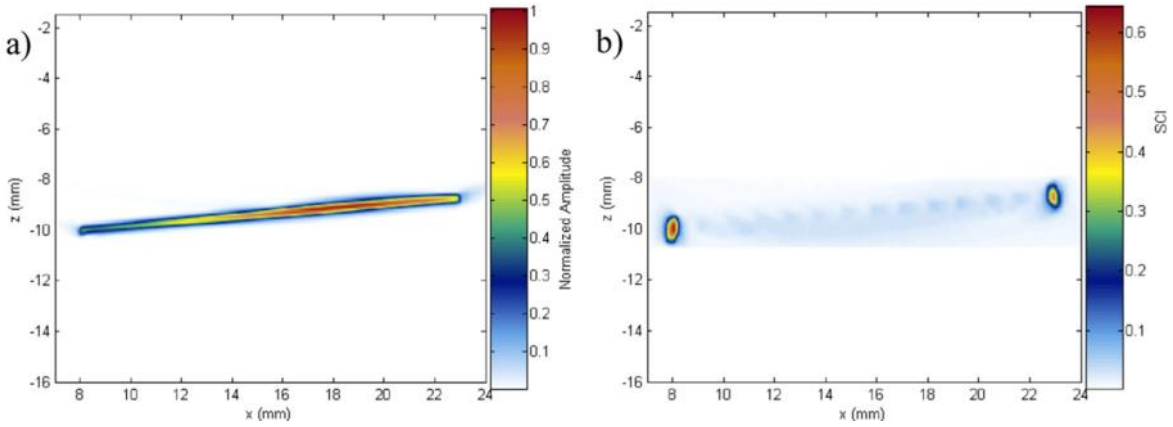

Figure 1-16. Ultrasound images of a plain fatigue crack using a) TFM and b) PCI [23]

TFM allows a single transducer to work as a transmitter, while all transducer elements receive ultrasound wave response. It produces a low-resolution image—further, another transducer element act as a transmitter. After the repeating process, all transducer elements are being used as a transmitter, which results in the creation of low-resolution images, which further are used for a high-resolution image. [23]

1.19. Phased array

The phased array method uses transducers, which is made from individual components, which could be driven independently. Probes are connected to adapted drive units, which allows to work independently, as well it enables simultaneous emission and reception through each independent channel. [28]
Variable geometry multi-element probes are being used for phased array method, however they must to meet requirements:

- Elements must work independently and without making vibration in nearby elements because of acoustic or electrical coupling.
- Every element performance should be as close as possible to confirm construction of homogenous beam.

Different possible geometry probes are shown in figure 1.17.

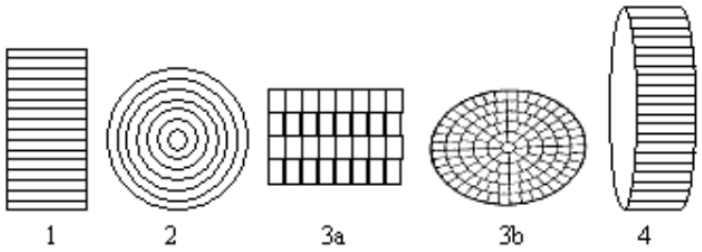

Figure 1-17. Examples of geometries of phased array transducer elements:

1. Linear array
2. Annular array with uniform pitch (non constant surfaces)
3. Matrix arrays (checkerboard and sectored rings)
4. Circular array [30]

Linear array probes are created from components, which are alligned along an axis. They allows beam to be focused, moved and deflected.
Annular array probes are made of set of rings. They allows to focus beam at different depths. Desiring focusing could be achieved, while each single element fires in different moment. Each ring surface is usually constant and each ring has different width. [29]
Circular array probes are created from set of elements, which are build in a circle. Elements could be directed to exterior, interior or along the axis. Usually mirror is used to adjust required beam angle.
Matrix array probes active area has 2 two dimensions in different elements. Matrix array probes allows the beam to be driven in 3D. [30]

In general, all probes offers more flexibility as single-element probes. All probes can be used in contact or immersion, probe can be focused or flat.

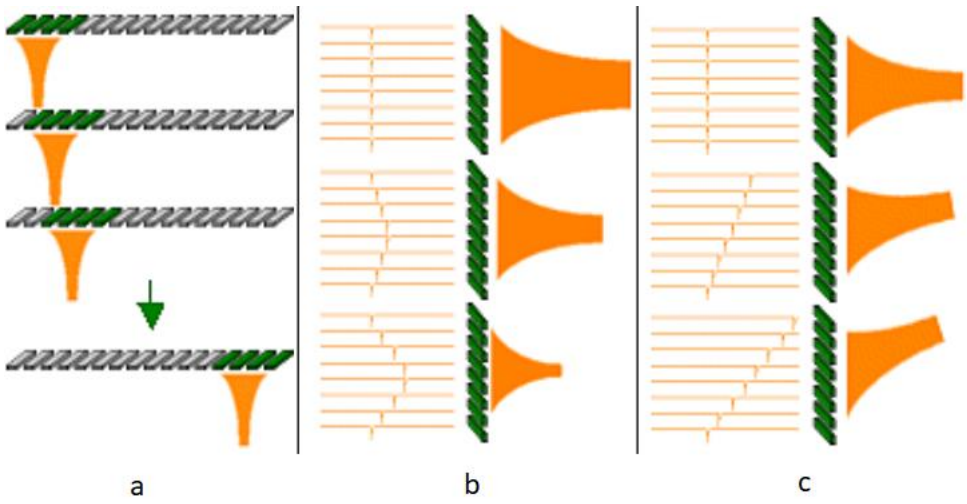

Figure 1-18. Indicated schematic of electronic scanning, focusing and deflection [30]

View of electronic scanning, focusing and deflection could be seen in figure 1.18. During electronic scanning group of elements are activated to move the beam with transducer. During electronic focusing delay laws could be applied to focus beam at desired area. Angle of the beam could be variated by delaying laws as well. [30]

1.20. Phased array annular probe design

It has been proved that phased array method with annular probe design is reliable method for micro cracks or any other damages inspection. The main reason why linear ultrasonic techniques are being replaced by nonlinear is due to acoustic effects, such as harmonic wave, which is sensitive to micro-cracks.
Phased array probes are classified as liner or annular, which depends on components position, as shown in figure 1.19.

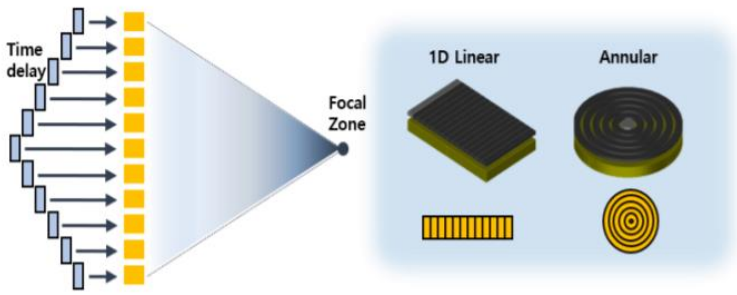

Figure 1-19. Schematic illustration of phased array beam focusing through time delay and two types of phased arrays [31]

One of the main features of phased array is electronic focusing and steering. Focal zone could be adjusted by time delay, which is determined and modified in each element as shown in figure 1.19.

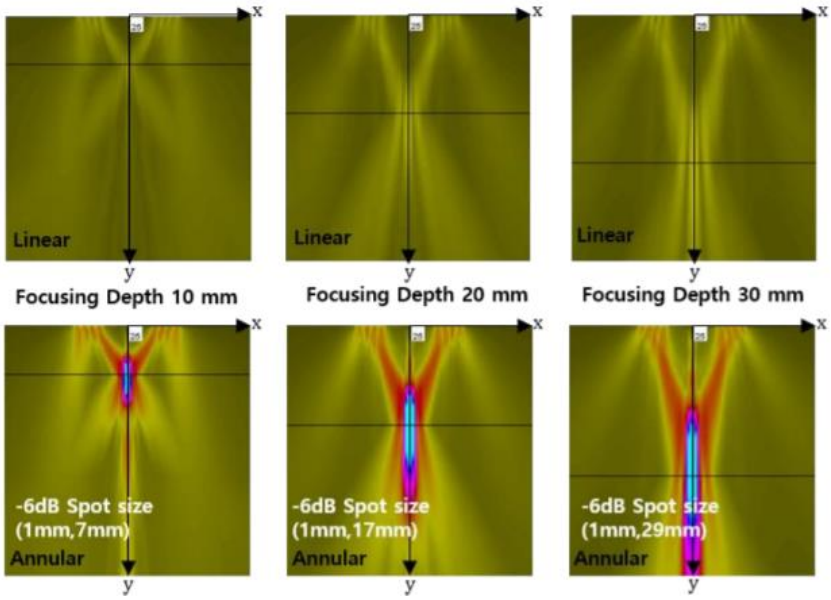

Figure 1-20. Beam focusing simulation results of the linear and annular phased arrays [31]

Seoul National University of Science and Technology has performed beam focusing simulation with linear and annular probes. As per figure 1.20. We can notice that, while using linear probe, beam focusing could be hardly noticed, however, using annular probe, beam focusing zone could be seen at three focal lengths. The reason for this is more efficient geometry of annular probe, while forming focused beam. [31]

1.21. Phased array method for crack detection

The phased array method could be used to detect various defects, including cracks in bolts. Instead of standard inspection, where the specimen is manually scanned via normal beams, and results are interpreted by the user, the below-described technique uses S-scan. The phased array probe is adjusted to the head of the bolt and performs S-scan down the bolt. The array probe is mounted in the encoded jig for 360-degree rotation. When the bolt is scanned from all directions, threads, all depths, and defects could be seen. S-Scan interpretation is more comfortable using this method. [32]

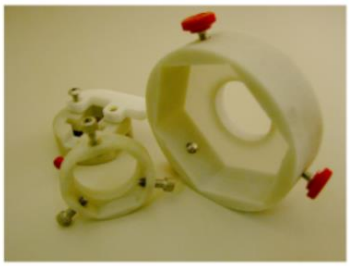

Figure 1-21. Small bolt jig base unit (left) and (right) large bolt jig [32]

During the inspection, an array is mounted on top of the bolt in the jig. Direct contact or wedge could be used, and however, if direct contact is used, a protective layer is needed. During calibration,

machined notches are introduced at bolt thread or any location where the crack is likely to happen. The beam goes through-bolt the body, threads, and end of the body, as shown in figure 1.22.

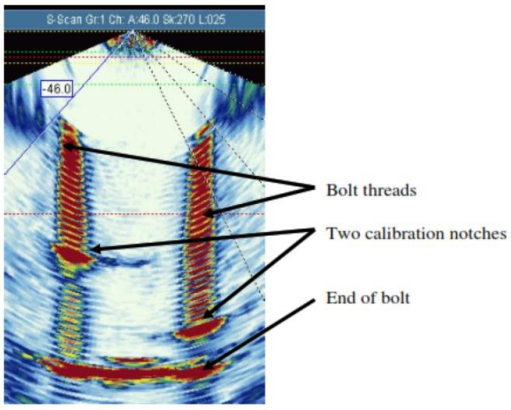

Figure 1-22. Scan of notched calibration bolt with threads. Notches and end of bolt labelled [32]

After S-Scan, all data is collected and stored, cracks, corrosion, or any defects recorded during the scan are stored and interpreted. [32] This method would be beneficial for commercial reasons. Scanned and stored data is easier to interpret, different setup options could be considered.

From research performed regarding possible NDT methods to be used for main landing gear tie-bolt inspection, phased array is considered to be most suitable. Phased array has the ability to control multi transducer elements independently. This option allows to steer the beam. While element pulse with time delays, beam focus could be generated at desired area. Phased array has high precision in defects detection and durations of inspection is not time consuming.

2. Main landing gear tie-bolt modelling in CIVA software

During the final thesis project, NDT inspection options available for the main landing gear tie-bolt were analyzed. Material and dimensions of tie-bolt were collected using available technical documentation. Approved tie-bolt NDT techniques were described. Analysis of the computer inspection model using CIVA NDT software was performed.

The main landing gear tie-bolt was designed using SolidWorks and AutoCAD software. 3D and 2D drawings were made and adjusted to be compliant with CIVA NDT software.

CIVA software provides the possibility to modify essential parameters involved in NDT testing, which is mandatory if there are need to determine the most appropriate NDT inspection method. Currently, CIVA provides five testing methods [33]

- Ultrasonic testing
- Eddy current testing
- Guided wave testing
- Radiography testing
- Computed testing.

CIVA allows stimulating all ultrasound inspection process with various probes, such as conventional, phased arrays, or EMAT. Almost all kind of specimens are available, since CIVA software support and allow to import CAD files. 2D and 3D simulation options are available. Materials of components could be metallic, fiber composites, or concrete. Many different flaws could be inserted into the specimen, such as calibration defects, planar defects, cracks, delamination, and more. [34]

Main features of CIVA UT analysis module [35]

- Classical images (A-Scan, B-Scan, C-Scan, D-Scan)
- The specimen could be reconstructed from simple to 3D.
- Industrial probes library
- UT Beam simulation
- Analysis procedures are automated.
- Complete traceability of actions performed.
- Full 3D data export
- Display in amplitude, depth, or time of flight.

2.1. Tie bolt material and geometry background

Broken tie bolt removed from DAT LT ATR aircraft, which was scrapped due to cracks found after NDT inspection could be seen in figure 2.1.

Figure 2-1. Main landing gear tie bolt

The technical specification indicates bolt material: Steel comp 8740 or steel comp 4140 or steel comp e4340 or steel comp 4340 or steel comp 6150.

Bolt dimensions designed as per military standard MS-21250. Dimensions in the below table 2.1 are in inches.[36]

Table 2-1. Bolt MS-21250 Technical specifications [36]

DIA DASH NO.	**THREAD MIL-S-8879**	**A DIA**	**B DIA**	**NOM SIZE W**	**D DIA**	**E MIN**	**H**	**J +.010 -..030**	**M**
06	.3750-24 UNJF-3A	.649 .639	.3745 .3735	.4375	.437 .422	.197	.388	.260	.070
DIA DASH NO.	**N DIA +-.005**	**Q**	**R**	**t min REF**	**U +-.016**	**GRIP +-.010**	**Length**		
06	.055	.091	.057 .047	.625	.047	2.375	3.020		

2.2. Simplified bolt model in CIVA

CIVA software UT module allows to creation simplified 3D specimen model. Specimens designed in SolidWorks or AutoCAD can be imported if the design form is more complex. The imported model must be edited and validated in CIVA to identify layers as the front wall, back wall, intersection. 3D Bolt was designed in SolidWorks and imported to AutoCAD to perform corrections on drawing lines.

The further 2D model was imported to CIVA and the model was validated. A detailed view of the simplified model could be seen in figure 2.2.
For the simplified model calculations method, focused transducer with a 9.51 mm diameter, 10 MHz flat focus transducer was selected. Notches, which are artificial defects for representing the cracks, were placed on the third complete root and in the incomplete thread root, as shown in figure 2.2. Focused transducer installed in the bolt inspection tank, where water path was set at 12 mm. Recommended water path is between 11,112 and 14,288 mm.

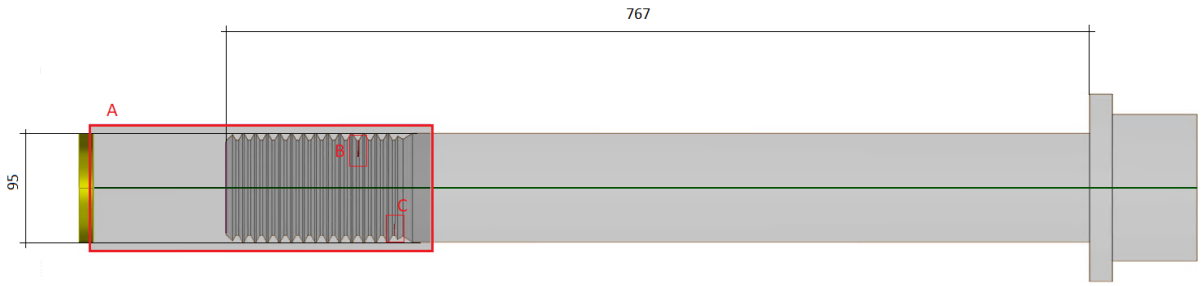

Figure 2-2. Simplified 2D Model view with two notches

As per the above figure 2.2, two flaws have been determined in the specimen. 2D surface-breaking flaw types were created. Both flaws are 3.8mm in length and 1 mm in height (refer B, C). Transducer computation zone A. Bolt diameter 95 mm and length 767 mm.

2.3. Defects positioning

There are many defect options in CIVA, where geometry, shape, size, and positioning could be determined. A scan will determine how amplitude changes versus time and will depend on defect position. Physical NDT inspection could verify calculations. Two defects in the bolt thread area were placed. [37]

2.4. Experimental set-up

During experimental set-up procedures in CIVA software, specimen, probe, inspection, flaws, and simulation settings features were used. Probe characteristics could be found in table 2.2.
For specimen, steel with longitudinal wave velocity of 5900 $m.s^{-1}$ and transverse wave velocity of 3230 $m.s^{-1}$ were selected. Material density was set to 7.8 $g.cm^{-3}$. During this experiment, attenuation was not taken into account.

Table 2-2. Probe characteristics determined in CIVA software

Probe type	Immersion
Crystal shape pattern	Signal element
Geometry shape	Circular
Geometry diameter	9.51 mm
Focusing surface type	Spherical
Surface radius	38.1 mm
Signal frequency	10 MHz

Probe was positioned on top of the bolt and inspection plane set by the side with positive inspection direction. The distance between the focused transducer and the bolt face was adjusted to give a water path of 12mm. Water as liquid couplant must be used to conduct the ultrasound waves between specimen inspected and probe selected. Water primary wave velocity – 1483 m. s^{-1}, density 1 $g.cm^{-3}$.

8 number of steps for focused transducer were determined. Each step set at 1 mm length along Y axis. As per figure 2.3 A shows step 0, and B shows step 8. Each step could indicate different A-Scan and B-scan, which allows to monitor defects amplitude depending on probe position, as well as threads positions, entry signal, back wall echo and other signals.

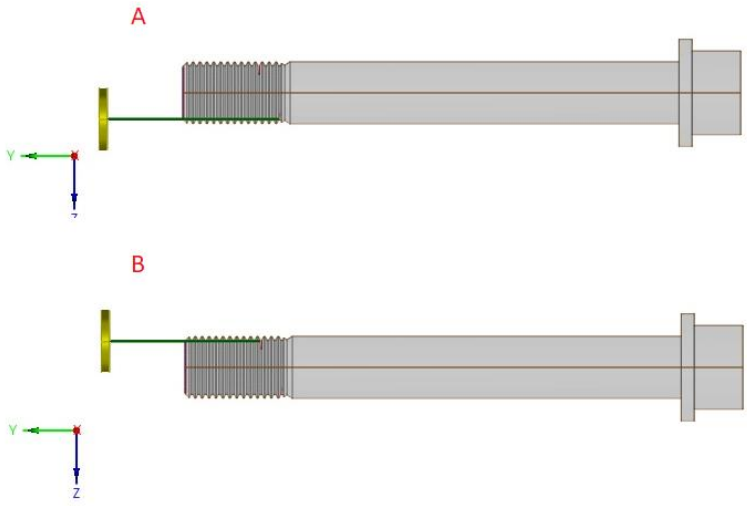

Figure 2-3. A) Transducer scan position 0 and B) transducer scan position 8

CIVA software allows to indicate accuracy, which by default is 1. It defines number of contributions calculated. In tie-bolt case to get more detailed results accuracy was set to 3.

2.5. Simplified ultrasound analysis

Two simulations have been performed in CIVA software. Flawless sample inspection and flaw detection simulation. During first simulation scanning of the bolt without the flaws to see the signal amplitude variations due to reflections from threads, without any flaws interfering was performed. During second simulation 2 flaws were introduced, which has been detected and compared.

2.6. Flawless defect detection

Scanning simulation without any flaws has been performed and A-Scan received. During flawless scan, transducer was configured to position as shown in figure 2.3(A). A-Scan could be seen in figure 2.4. During flawless bolt scan signal reflection from the threaded area, back wall echo and entry signal were obtained.

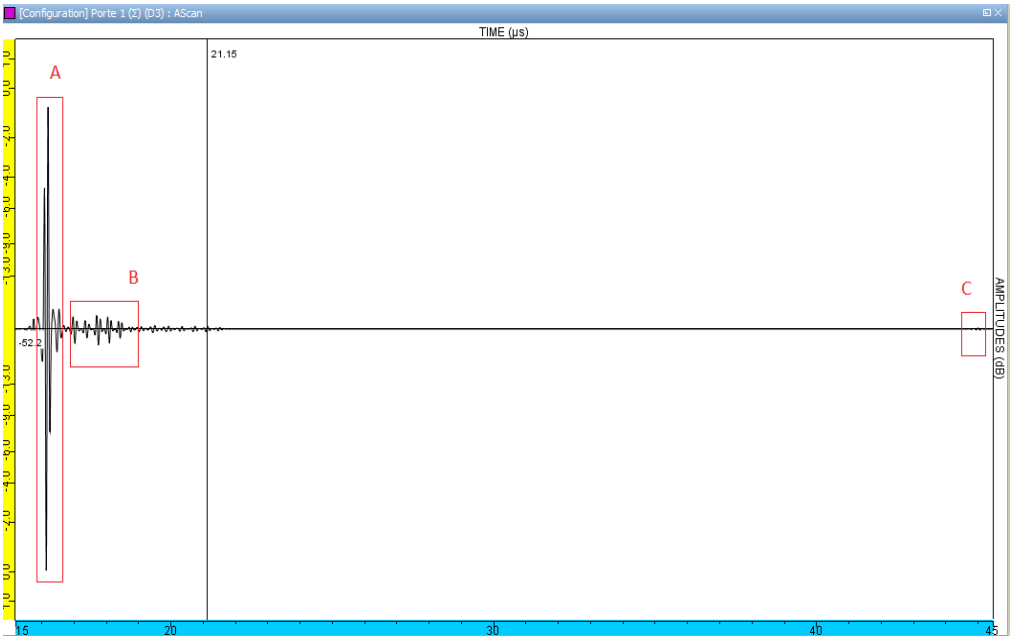

Figure 2-4. Flawless A-Scan of bolt

Below points could summarize figure 2.4:
A – Surface reflection; B – signal reflection from the threaded area; C – Back wall echo.
No other signals have been detected.

2.7. Flaw detection

The surface breaking flaw size that was tried to be detected was 3,8 x 1 mm and located at the third complete thread root area. As it could be seen in figure 2.6, a defect A-Scan was obtained, when probe was located at probe position shown in figure 2.5.

Figure 2-5. 3D Scan right view, defect at the third complete root area and placed notch (A)

A-Scan when probe located at number 7 scanning step could be seen in figure 2.6. Notch type defect, which could be seen at peak C were detected. In the A-Scan, presented in figure 2.6. Following signals can be identified:

A – Peak at the entry to bolt; B – signal reflection from the threaded area; C- Defect reflection.

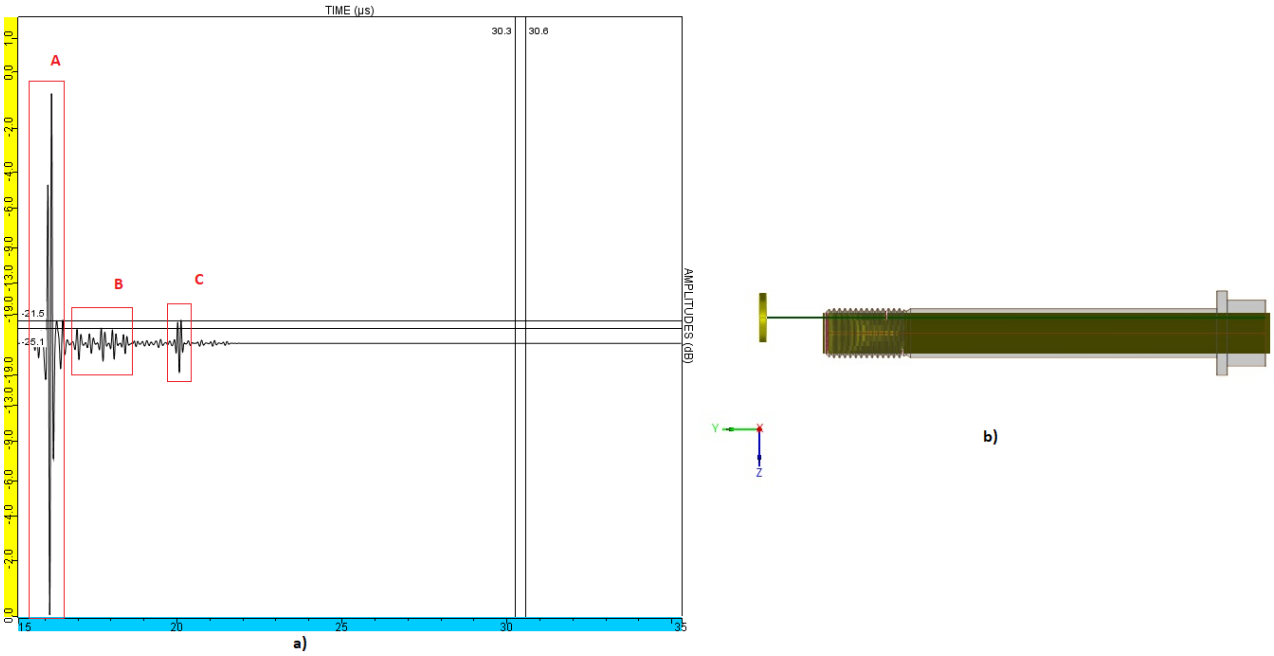

Figure 2-6. a) A-Scan time and amplitude graph of the bolt with defect at the third complete thread root area; b) probe position

As per figure 2.7. It could be noticed that maximum amplitude from threaded area is -25.1 dB and maximum amplitude from defect reflection is -21.5 dB

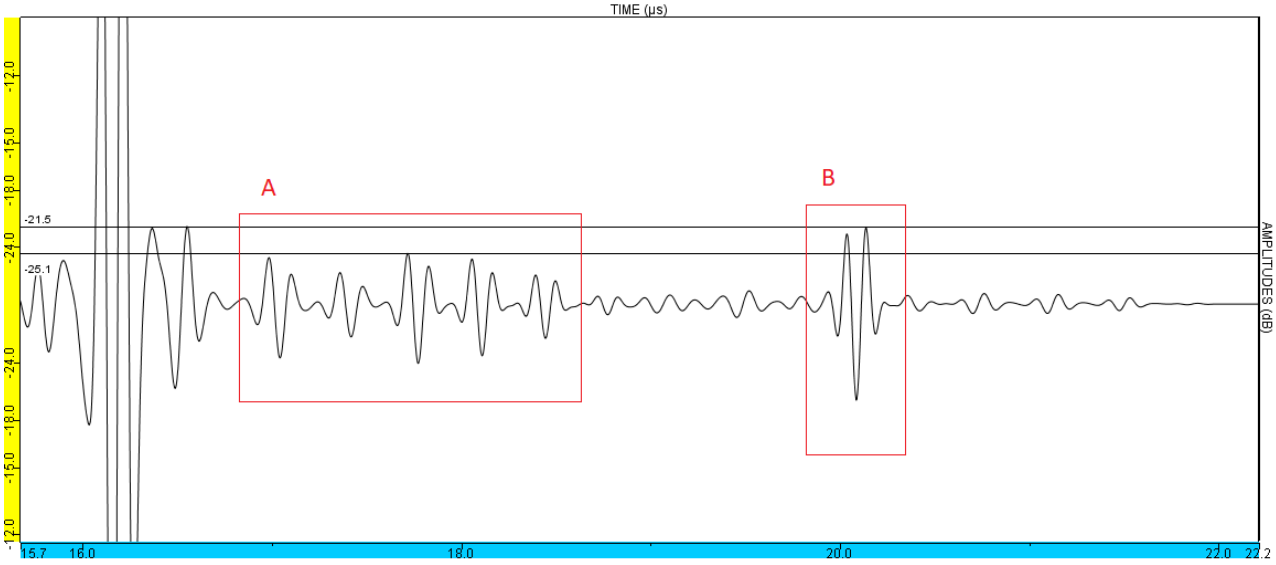

Figure 2-7. Threaded area amplitude against reflect from defect amplitude

The second surface breaking flaw size that was tried to be detected was 3,8 x 1 mm and located at first incomplete thread root area as shown in Figure 2.8.

Figure 2-8. 3D scan view, defect at the incomplete thread root area and placed notch (B)

A-Scan was obtained when probe was located at position shown in figure 2.9. Placed defect were detected and could be seen at peak C. From below figure 2.9, three points could be summarized:
A – Peak at the entry to bolt; B – signal reflection from the threaded area; C- Defect reflection.
No other signals have been detected.

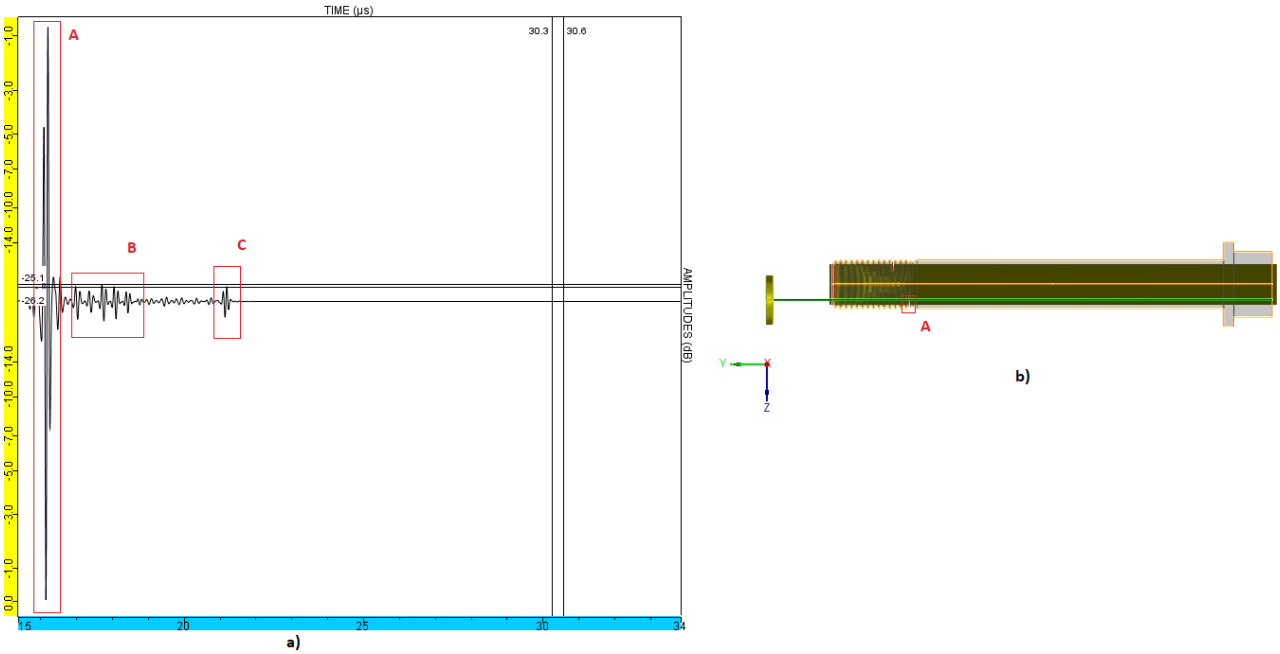

Figure 2-9. a) A-Scan of the flaw at the incomplete thread root area b) probe position and defect position (A)

As per figure 2.10, it could be noticed that maximum amplitude from threaded area is -25.1 dB and maximum amplitude from defect reflection is -26.2 dB.

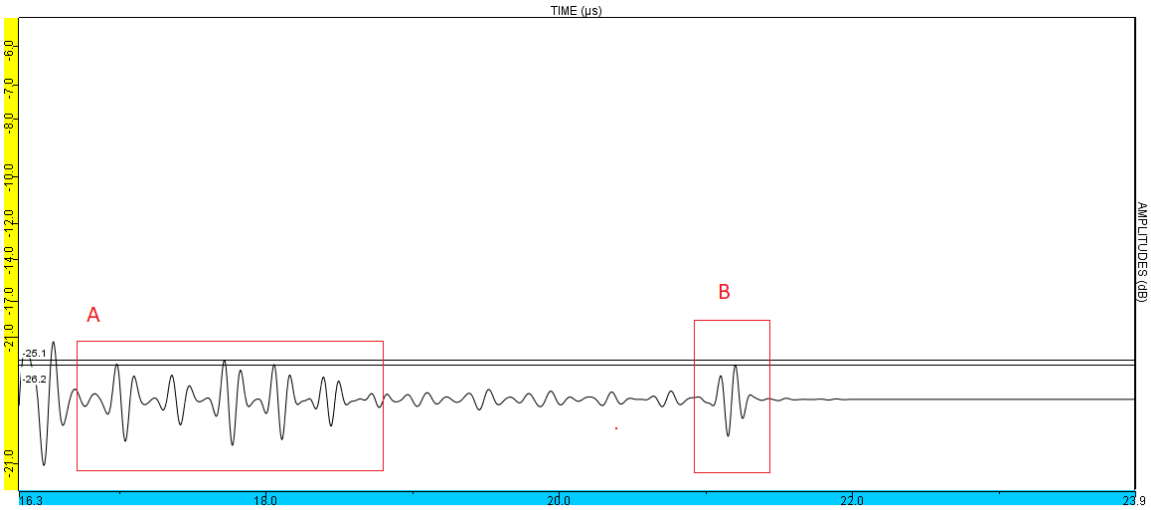

Figure 2-10. Maximum amplitude from the threaded area and defect reflection

In terms of amplitude the difference between threaded area and defect is very similar. Due to similarity, it would be difficult to detect the defect.

2.8. Simplified models graph comparison

Figure 2.11 indicates combined graphs of A-Scan with defects in the third complete root thread area and A-Scan without defects at the mentioned area. It could be seen that both graphs are identical except point C, which describes the defect found.

A – Peak at entry to bolt; B – signal reflection from threaded area; C- Defect, D – Back wall echo. No other signals have been detected.

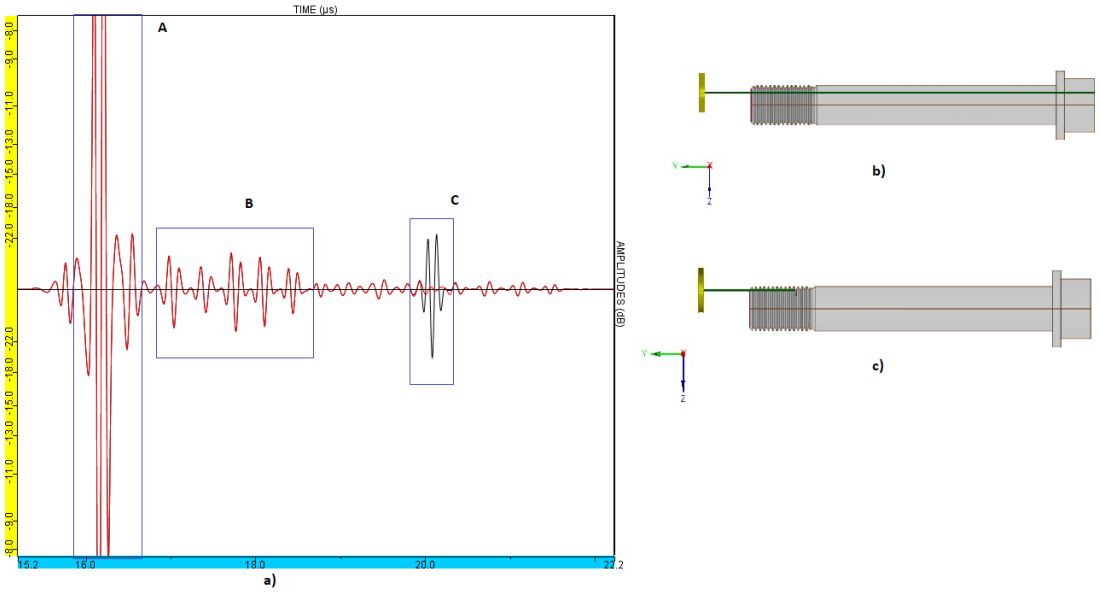

Figure 2-11. a) A-Scan of defect at threaded area comparrison against scan without defect; b) bolt scanning without notch placed c) bolt scanning with notch placed in threaded area

Figure 2.12 indicates combined graphs of A-Scan with defects in incomplete root thread area and A-Scan without defects at the mentioned area. It could be noticed that both graphs are identical except point C, which describes the defect found. Comparing A-Scans, it could be seen that the defect located at the third root area could be noticed further in time domain.

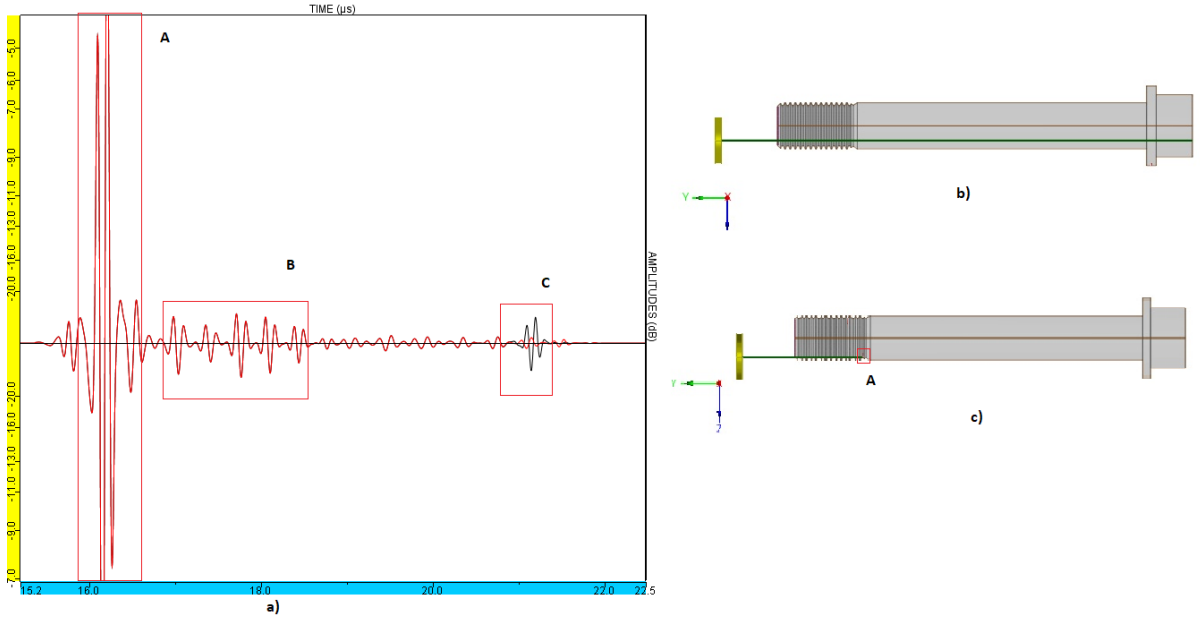

Figure 2-12. a) A-Scan of defect at incomplete thread root area against scan without defect. b) bolt scan without notch placed. c) bolt scan with notch placed (A)

A – Peak at entry to bolt; B – signal reflection from threaded area; C- Defect, D – Back wall echo. No other signals have been detected.

2.9. Beam focusing

During non-destructive testing immersion analysis, 12mm water path were selected as per manufacturer recommendations. Water path helps to adjust beam focusing area. Beam computation simulation was performed to determine focal point location in designed specimen. [38]

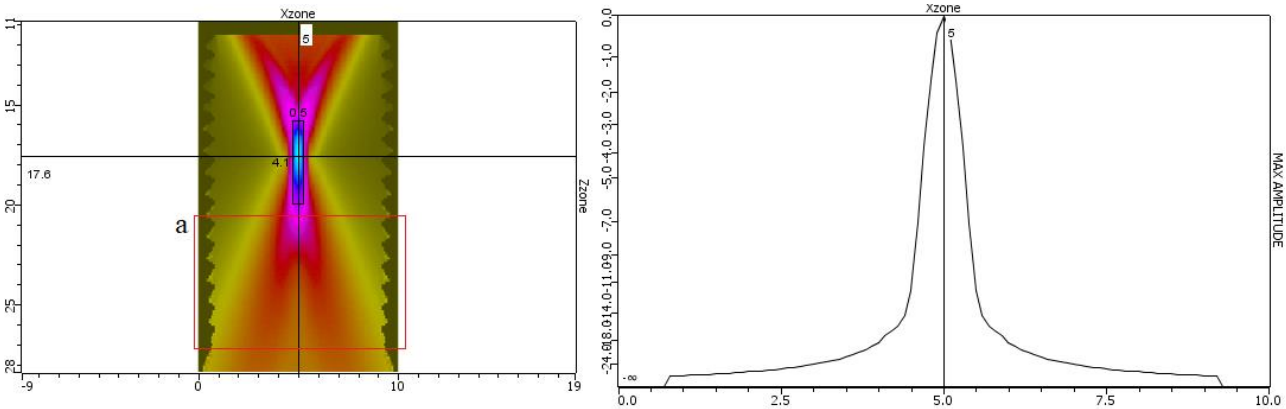

Figure 2-13. Focused immersion 10MHz probe acoustic field and zone of interest (a).

As per figure 2.13 it is noticed that beam focusing focal point is 4.1 mm length and 0.5 mm. It is known that most critical part of the bolt is incomplete first thread root area and third or fourth complete thread root area. Mentioned areas are zone of interest, however beam focusing scan indicates that focal point does not reach mentioned areas. Current determined focal point covers 7-11th thread root area.

2.10. Parametric studies

One of the main CIVA software features are parametric studies, where the user defines the parameters and values which will vary. Parametric studies enable to estimate variation of amplitude of a signal, reflected from defect, when the size, position, or angle of defect changes. Every different variation provides with different A scan and 3D view, where variable reflects. [39]
In total 3 different variation calculations were performed: flaw angle, flaw height and position.

2.11. Defect position variation

To have a view of A-Scans, when defect is positioned on complete thread root area, 14 variations on each threaded area was performed. Each step between threaded area was calculated 1.059 mm. Investigations discussed previously and manufacturer recommendations suggest that most critical areas are first incomplete thread root and third or fourth complete thread root area. To understand how reflection from threaded area will influence the results, it was decided to analyze how A-Scan will depend on:

- Flaw located at most critical area, first incomplete thread root.
- Flaw located at beam focal point position; 7th threaded root area.
- Flaw located at the last thread.

First, probe was positioned as shown in figure 2.14 and calculations were performed, when notches are located at first threaded root area, 7th threaded root area and last thread.

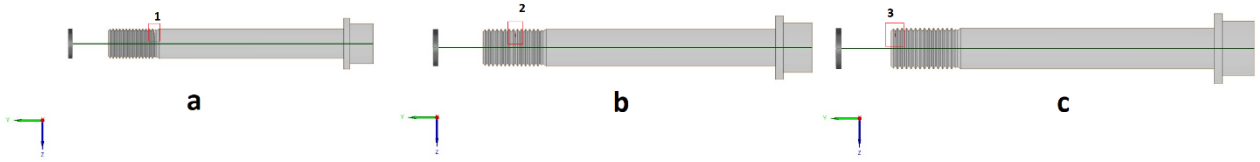

Figure 2-14. Probe position on center and parametric notches on a) first incomplete thread root b) 7th threaded root area, and c) last thread.

After parametric calculations, three A-Scans of most interested areas were extruded and combined in single A-Scan to see a difference in amplitude. Notch located at first incomplete thread root area were marked in black, notch in 7th thread is marked in green and notch in last thread is red. From below figure 2.15, it could be noticed, that if probe is located as shown in figure 2.14, it's difficult to identify the defects due to threads reflection. On 7th thread area, where focal point exists, slight difference in

amplitude could be seen, however without knowing this notch, it would be extremely difficult to interpret this area as cracked since threads reflection amplitude is same.

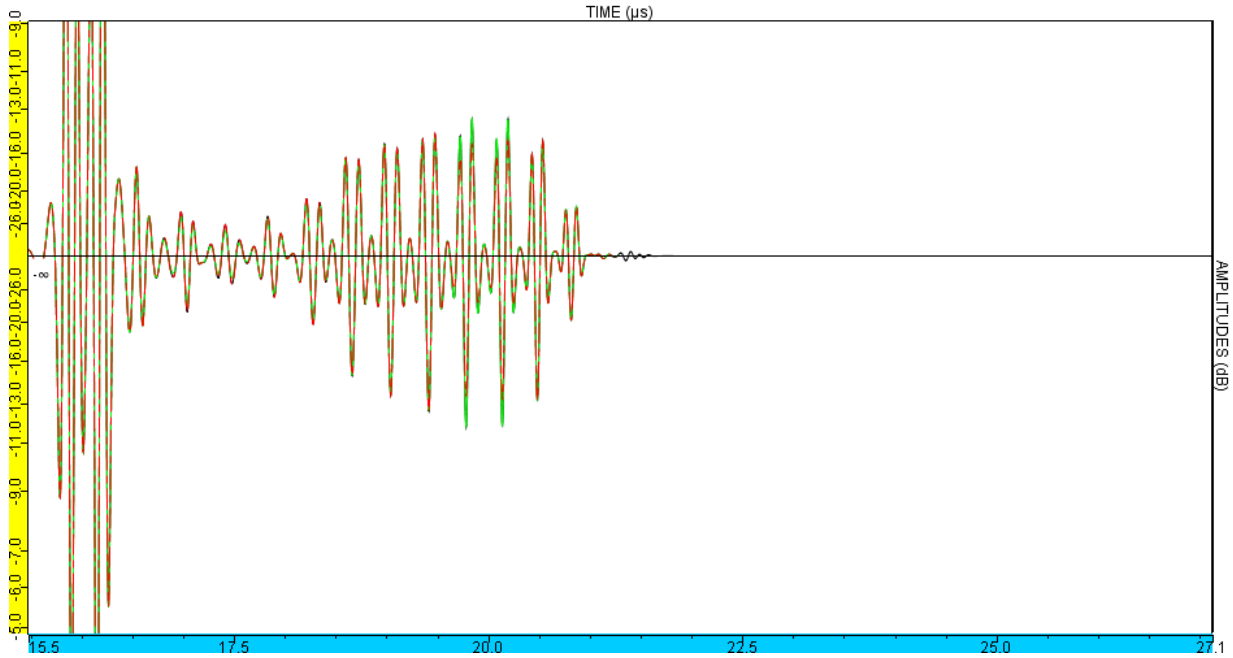

Figure 2-15. A-Scans of the threaded area. Black – first incomplete thread root area; green – 7th threaded area; red – last thread

Afterwards, probe was placed as shown in figure 2.16 and identical calculations performed.

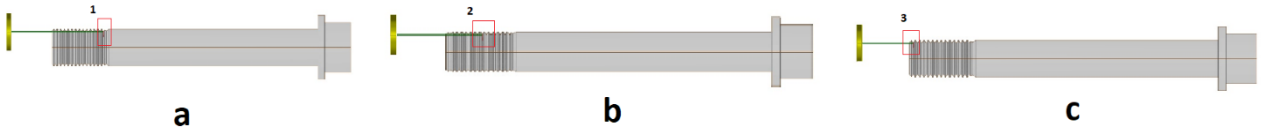

Figure 2-16. Probe position and notches on a) first incomplete thread root, b) 7th threaded root area, and c) last thread

From A-Scans received and combined as shown in figure 2.17 it could be noticed, that when probe is positioned parallel to threads, notched could be identified. Defect located on 7th thread root area is located at focal point of the beam and has highest amplitude at -18.5 dB. Defect located at most critical first incomplete thread root area is not in the beam focal point range and A-Scan amplitude is lowest at -32.7 dB. A-Scan from notch located in last thread could be seen in figure 2.17 and is marked in red. It could be discussed that without knowing exact notch location, it would be very difficult to interpret the defect.

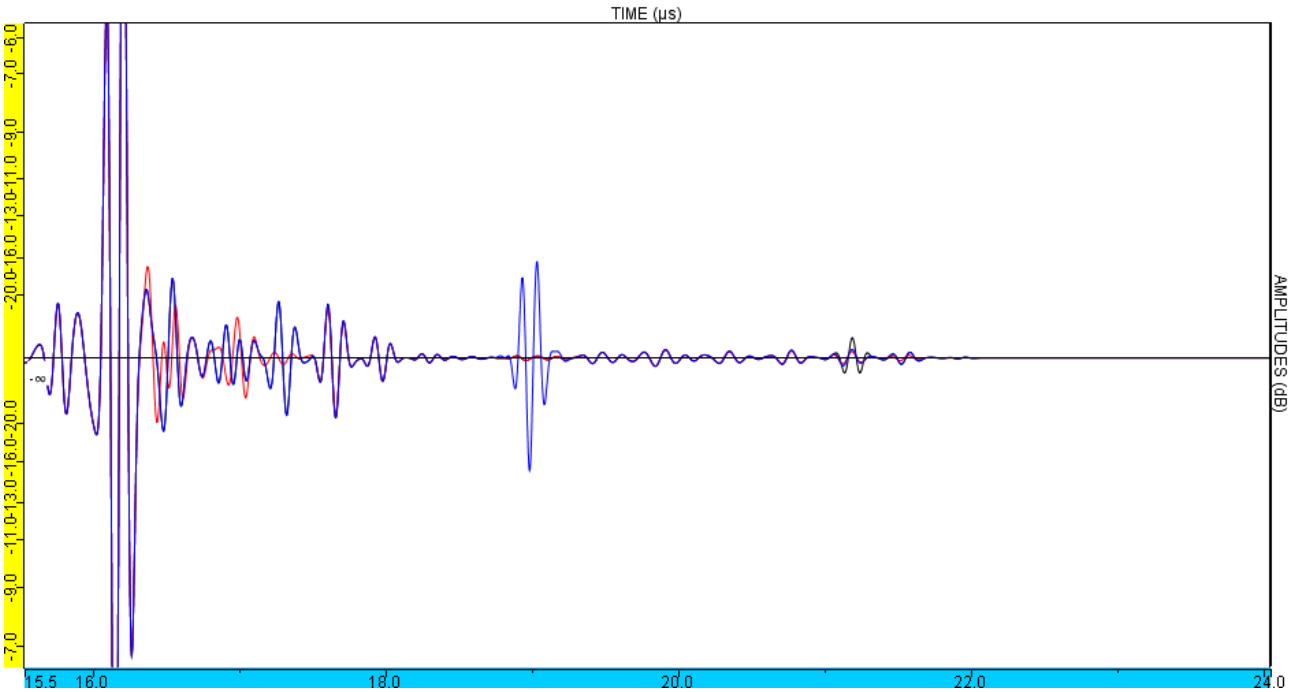

Figure 2-17. A-Scans of defects position variation

After parametric studies performed when defect position variates between first and last thread and probe positions are different, it could be concluded that the best view of defects could be noted, when probe position is parallel to threaded area and notches are in focal point area. When probe is located at center area, amplitudes are almost identical independent where the notch are located.

2.12. Defect flaw variation

Defect flaw variation calculation were performed on forth complete thread root area. In total 25 number of variations were calculated, starting from 0,1mm to 5mm. Each step between flaw height during variation computation was 0,204 mm.
After all A-Scans received and analyzed it was selected to combine and compare A-Scans of following variations:
Notch 1: 0.1 mm height.
Notch 2: 0.3 mm height.
Notch 3: 0.5 mm height.
Notch 6: 1.1 mm height.

Below figure 2.18 indicates mentioned notches variation of A-Scans combined. It could be noticed that if probe is positioned at specimen center area, any difference could be seen in notch amplitude due to high amplitudes in threads reflection.

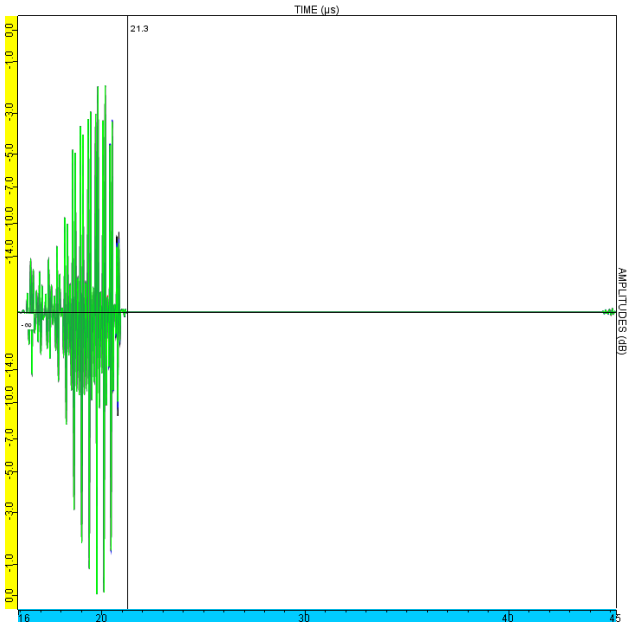

Figure 2-18. Combined A-Scans with flaw size of a notch at the fourth complete thread root area, when probe positioned at specimen center area.

Defect flaw height variations at critical forth complete thread root area was performed. Initial configuration of defect height was set to 0.1 mm. In total 25 number of values of 0.204 mm step were calculated. As shown in figure 2.19 A-Scans were combined. It could be noticed that without knowing position of defect, identification, when defect is up to 0.3mm would be difficult. Inspector could interpret that defect exist when defect flaw is starting from 0.5 mm.

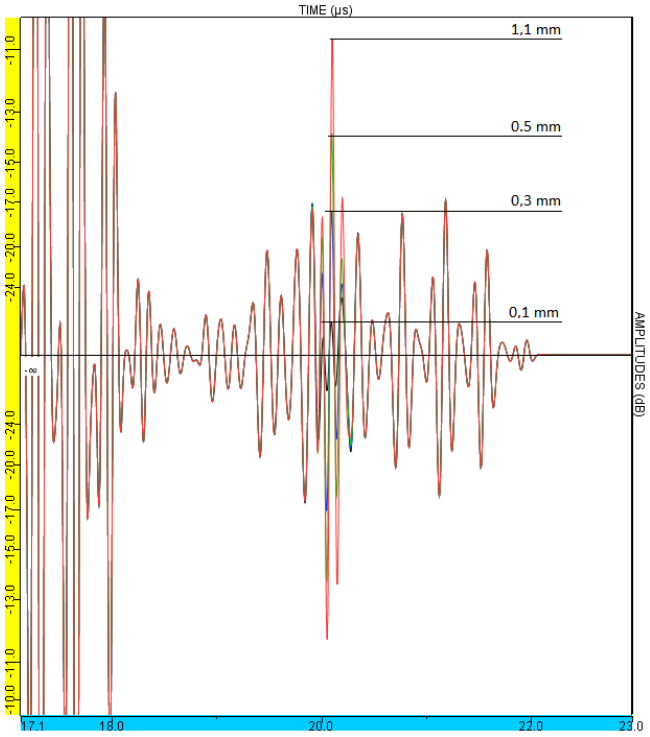

Figure 2-19. Combined A-Scans with flaw size of notches at the fourth complete thread root area, when probe positioned in parallel to the threaded area

After comparing results of A-Scans when probe is located at different positions and flaw height variates, statement could be made that if probe is located at specimen center position, it is difficult to identify notches due to high amplitude of threads reflection. If probe is positioned in parallel to threaded area, it could be possible to identify notches in A-Scan, however without knowing exact position of notches, all defects below 0.5 mm height would be difficult to identify due to high amplitude of threaded area reflection.

2.13. Angle variation

The reason to perform angle variation computation is to determine if there are any possibility to detect defects, which are located not directly with transducer beam, but on the other side of the bolt as well. Angle variation was performed on forth complete thread root area. 10 variations were performed starting from 0^0 to 90^0, every step was set at 10^0 . 2 different probe positions were selected: probe parallel to threaded area and probe positioned at bolt center area.
After all A-Scans received and analyzed, it was selected to combine and compare A-Scans of following variations:
Notch 1: 0^0 degree.
Notch 4: 30^0 degree.
Notch 6: 50^0 degree.
Notch 10: 90^0 degree.

Below figure 2.20 indicates variation of angles on specimen.

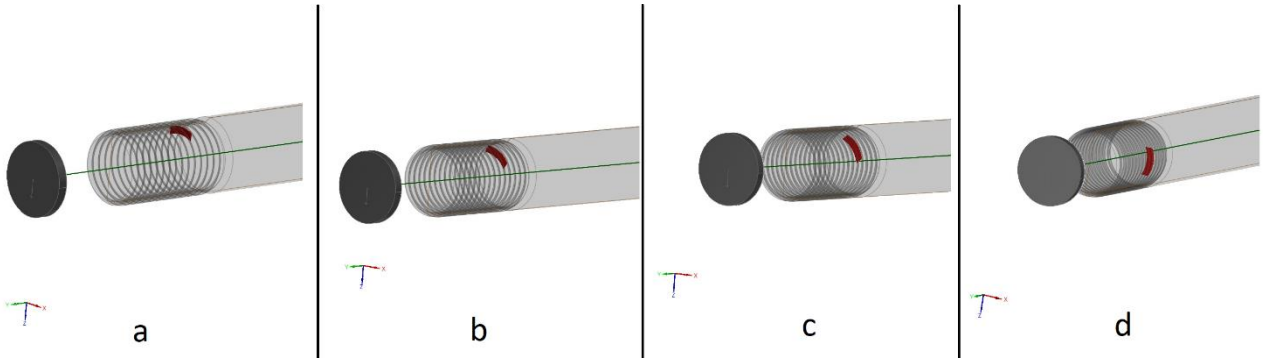

Figure 2-20. Angle variation

Parametric studies when notch angle variates between 0^0 and 90^0 and probe are positioned at center specimen area was performed and could be seen in figure 2.21. It could be noticed that independently from angle, no difference in A-Scans could be noted. Only threads reflection is visible.

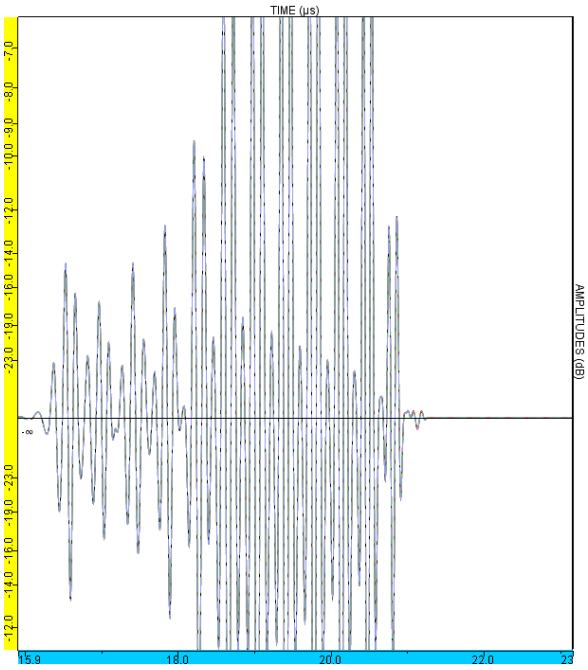

Figure 2-21. A-Scans of defect angle variation from 0^0 to 90^0, when probe positioned on specimen center area

Further studies A-Scans, when probe is located in parallel with threaded area could be seen in figure 2.22. A-Scan represent 4 different angle variations:
Black amplitude – 0^0.
Red amplitude – 30^0.
Green amplitude -60^0.
Blue amplitude – 90^0.

It was noticed that notch located at 0^0 could be identified from A-Scan without knowing the defect position. For inspector, it would be difficult to interpret defects located at 30^0 ,60^0 and 90^0 without knowing exact location, since reflection from threads amplitude is higher or same then notch amplitude. Every angle which is further from probe has lower amplitude, the reason of this is focal point area, which is parallel to beam.

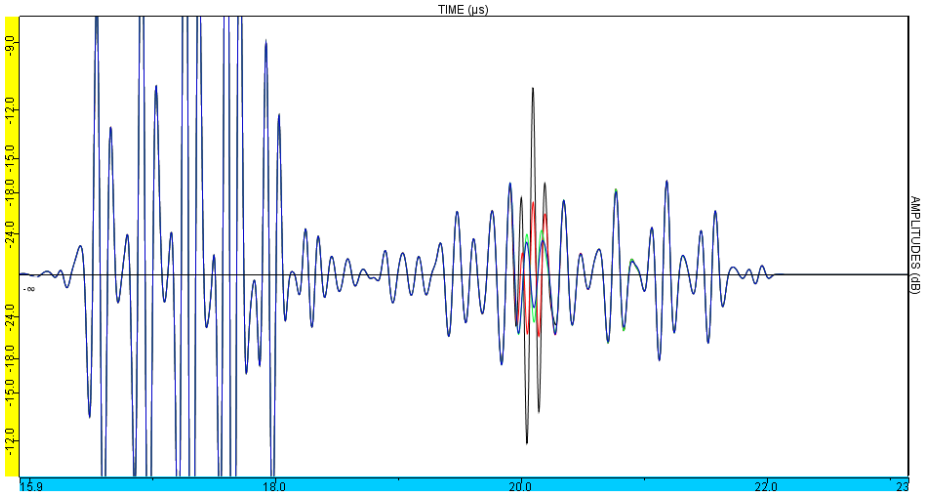

***Figure* 2-22.** A-Scans of defect angle variation from 0^0 to 90^0, when probe position area parallel to the threaded area. Black amplitude – 0^0. Red amplitude – 30^0. Green amplitude -60^0. Blue amplitude – 90^0.

3. Development of matrix phased array for tie-bolt analysis

Previously currently existing ultrasound immersion method applied on aircraft main landing gear tie-bolts and their flaw detection was analyzed. It was found that:

1. Existing method beam focal point does not cover most critical areas on first incomplete thread root area and third/forth complete thread root area.
2. High amplitude of threads reflection does not allow to interpret flaws correctly without knowing exact flaw position.
3. Mechanical scanning is required.
4. If defect are not located in focal point area, height, flaw location and angle variations proved that in many cases defects could not be interpreted correctly without knowing exact flaw location.

Due to reasons above it was decided to develop more advanced method for flaws detection in tie-bolts. Matrix phased array method consists of many transducer elements, which can be controlled independently. This option allows to focus beam or steer the beam axis. While element pulse with different time delays, we have an option to generate beam focus at desired area, which would offer higher flexibility for operator. Ability to perform electronical scanning, while using matrix phased array would be huge advantage over mechanical scanning. This method would allow to interpret defects at higher rate and would reduce human error, which could be made while interpreting the defect or its location. [40]

3.1. Phased array set-up

During experimental set-up procedures in CIVA software, following features were used: specimen, probe, inspection, flaws, and simulation settings. Matrix phased array characteristics could be seen in table 3.1.
For specimen, steel with longitudinal wave velocity of 5900 $m.s^{-1}$ and transverse wave velocity of 3230 $m.s^{-1}$ were selected. Material density was set to 7.8 $g.cm^{-3}$. During this experiment, attenuation was not taken into account.

Table 3-1. Matrix phased array characteristics determined in CIVA software

Probe type	Contact
Crystal shape pattern	Matrix phased array
Incident dimension	8.15 mm
Orthological dimension	8.15 mm
Number of elements in row	16
Number of elements in collumn	16
Gap between elements of a row and column	0.01 mm
Width in indicent and orthogonal plane	0.5 mm
Signal frequency	10 MHz
Surface type	Flat

Probe was positioned on top of the bolt at center and inspection plane set by the side with positive inspection direction. In current case no number of steps were selected, since current configuration allows to position focal point at desired area. Beam angle could be adjusted. Probe position shown in figure 3.1.

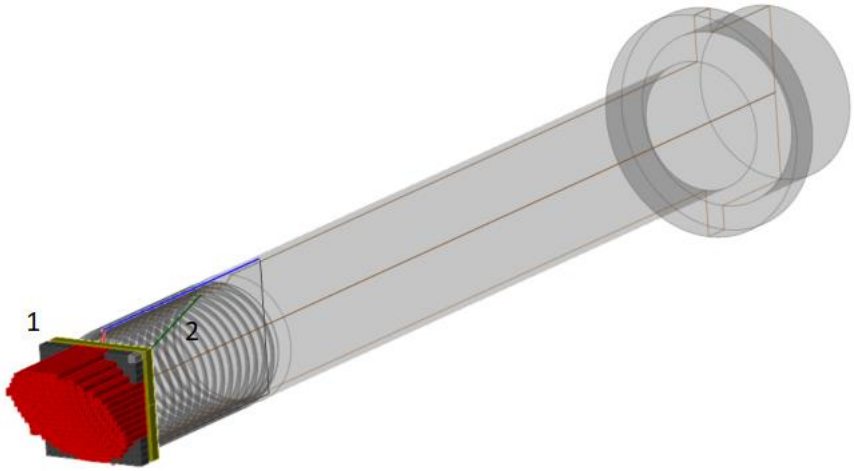

Figure 3-1. Matrix phased array on top of the bolt at center area. Delay laws (1), focused beam (2)

3.2. Beam focusing

During matrix phased array development, first goal was to calculate beam focal zone and to manage focal zone position in specimen. During first computation, beam configuration to target third and fourth complete thread root area was performed. As per figure shown in figure 3.2 it could be noticed that focal zone covers mentioned threaded areas and current focal zone is 0.9 mm width and 6.2 mm length, which is almost twice bigger than focal zone calculated, while using immersion method.

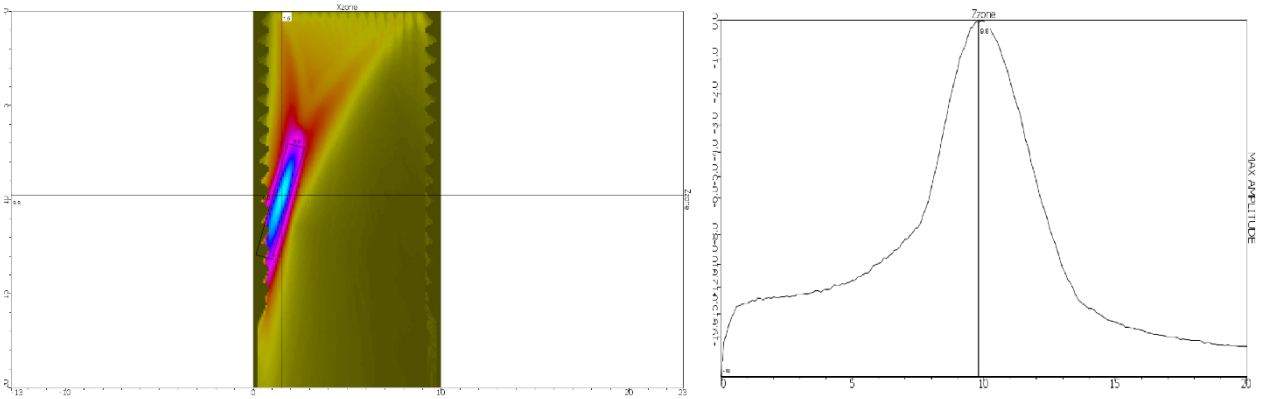

Figure 3-2. Matrix faced array 10MHz probe acoustic field

After successful focal point calculations, it was decided to change beam direction to second critical area – first incomplete thread root area and to change focal point location to desired location. Computation after beam location changed is shown in figure 3.3 it could be noticed that after re-

positioning beam, focal point on desired area were achieved. Calculated focal zone is 1mm width and 8.2mm length, which is twice bigger than calculated with immersion method.

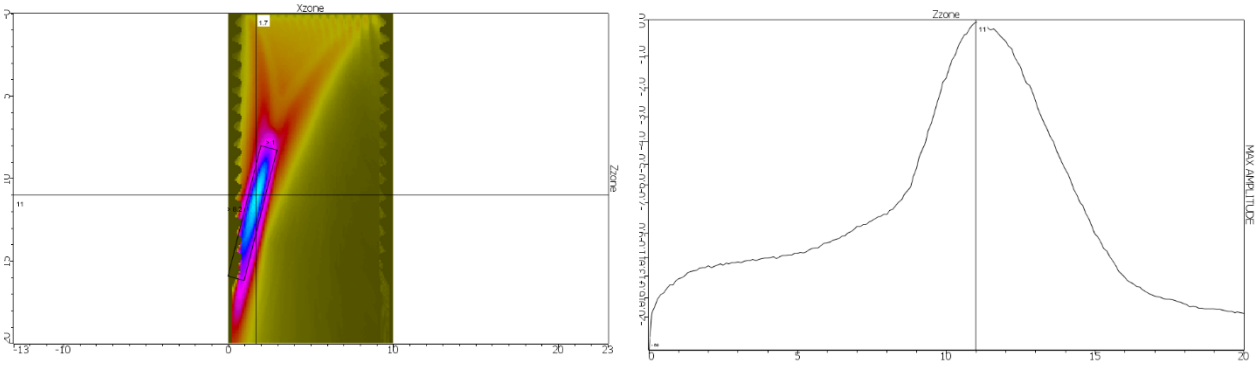

Figure 3-3. Repositioned beam matrix faced array 10MHz probe acoustic field

Both calculations shows that focal point could be adjusted and changed electronically without moving probe with matrix phased array method. Ability to change focal point, provides high flexibility in further calculations. Independently from flaws variation, with current focal zone there are better ability to clearly identify created flaws.

3.3. Flaw detection using matrix phased array probe

After beam computation and focal point detection, 2 surface breaking flaws were added as shown in figure 3.4. Defects characteristics were described at chapter 2.3.2 Flaw detection.

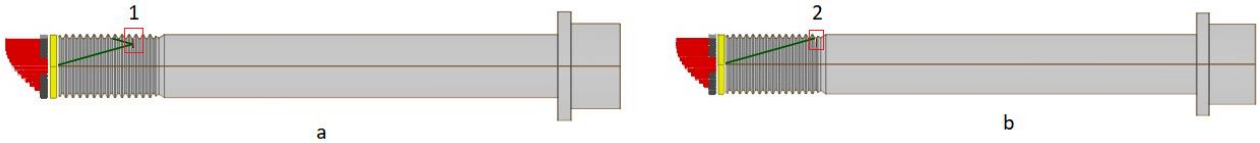

Figure 3-4. a) defect (1) at fourth complete thread root area; b) defect (2) at first incomplete thread root area

After calculations, both breaking flaws A-Scans were obtained, and defects found as shown in figure 3.5. Below points could summarize A-Scans.

A – Peak at the entry to bolt; B – signal reflection from the threaded area; C – Defect reflection. D – back wall echo.

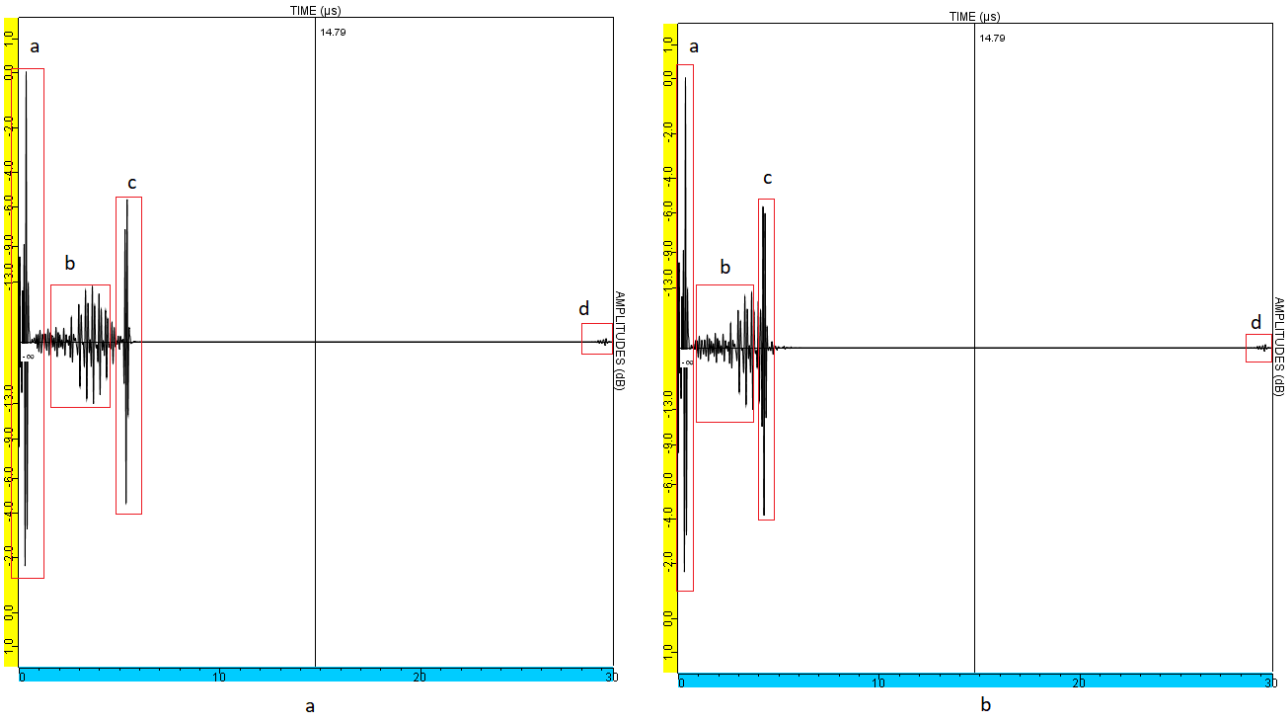

Figure 3-5. a) A-Scan of defect at forth complete thread root area. B) A-Scan of defect at first incomplete thread root area

Both A-Scans were compared as shown in figure 3.6. Black graph represents A-Scan, where notch is located in first incomplete thread root area and red graph represents graph, where notch are placed in forth complete thread root area.

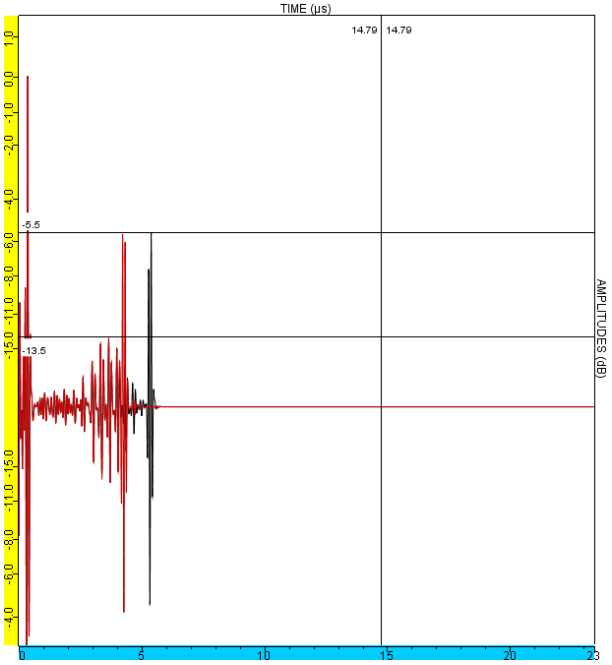

Figure 3-6. Combined A scans of defects placed in first and fourth thread root area

Both defects were 3.8mm length and 1mm height, which is the reason that both notches amplitude are same -5.5 dB. Reflection from threads amplitude is -13.5 dB. Both notches are clearly visible on A-Scan and could be interpreted without knowing where the defect are.

3.4. Matrix phased array parametric studies

For further analysis, parametric studies performed, where flaw position, angle, and height variates. Probe positioned on specimen center area. To justify this method flexibility and to be able to compare both methods following variations of defect performed:

1. Defect position variation. 14 variations on each threaded area. Each step between threaded area was calculated 1.059 mm. Due to most critical areas are first incomplete thread root and third/forth complete thread root area it will be area of interest.
2. Defect height variation. In total 25 number of variations was calculated, starting from 0,1 mm to 5mm. Each step between flaw height during variation computation was set to 0,204 mm. For further methods comparison 4 defect variations were used: 0,1 mm, 0,3 mm, 0,5 mm, 1,1 mm.
3. Defect angle variation. 10 variations were performed starting from 0^0 to 90^0, every step was set at 10^0. For further comparison, defects location was set at: 0^0, 30^0, 50^0, 90^0.

Differently from immersion method analysis, all calculations are performed electronically, when transducer elements are fixed at center position. For defect position variation and defect height variation, electronical scanning is performed. A-Scans will show defects, since after beam focusing on specific angle and depth, reflection amplitude received will be higher than reflection from threaded area. During defect angle variation, matrix phased array capability to steer the beam axis was used.

3.5. Matrix phased array defect position variation

From computation results, 3 A-Scans were extruded and combined, where 1st notch was located at first incomplete thread root area, 2nd defect located at 7th complete thread root area and 3rd notch at last thread root area.

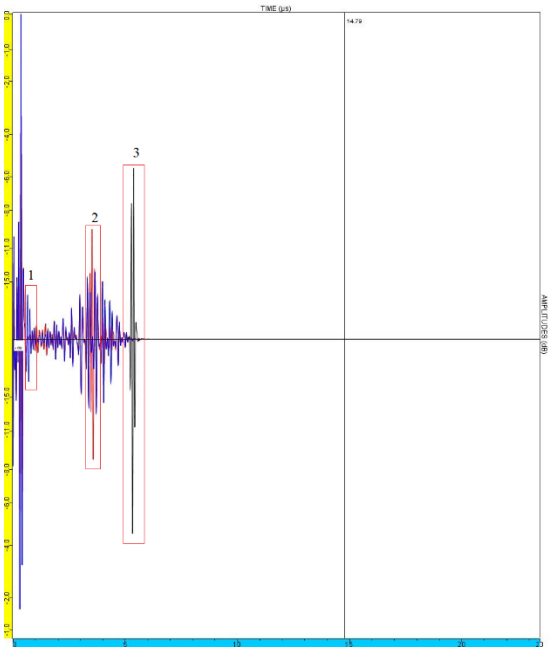

Figure 3-7. Matrix phased array defect position variation

As per figure 3.7, it could be noticed that defects located at first incomplete thread root area and 7th complete thread root area have much higher amplitude against threaded area. Measured amplitudes:
First incomplete thread root area -5.6 dB.
Seventh complete thread root area – 9.4 dB.
Last complete thread root area – 17.3 dB.
Threaded area – 14.3 dB.

From measured amplitudes it could be seen that defect positioned in last complete thread root area could not be interpreted without knowing exact position of defect, since A-Scan amplitude is lower than threaded area amplitude, however for such case, developed method would provide a capability to change beam and focal zone location as shown in figure 3.8.

Figure 3-8. Delays law adjusted (1) and beam position adjusted (2)

A-Scan obtained has confirmed that after beam position and focal points adjustment defect could be clearly visible on A-Scan as shown in figure 3.9.

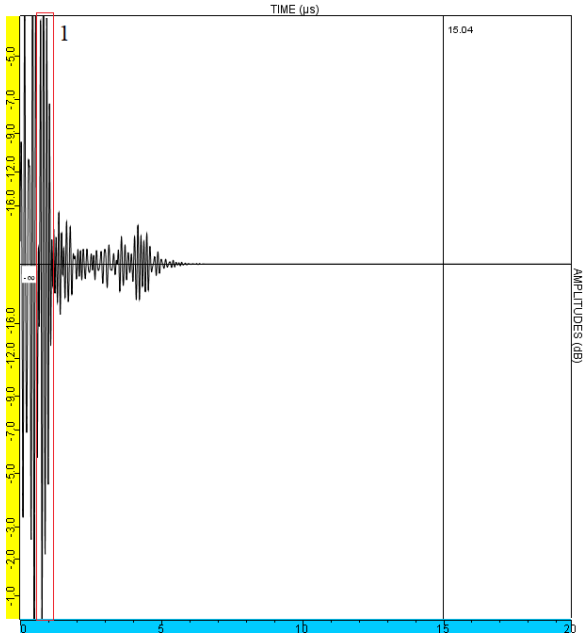

Figure 3-9. A-Scan of defect located at last complete thread root area

Although defect located in last complete thread root area are not likely to happen as per previous analysed events in DAT history, however option to steer the beam would allow to inspect it in case of need.

3.6. Matrix phased array defect flaw variation

For defect flaw variation computation, it was decided to compare 4 results, which would indicate, lowest possible detection height as on previously analyzed immersion method. The results could be seen in figure 3.10. It could be noticed that only 0,1 mm defect could be difficult to interpret due to threaded area reflections. Defects from 0,3 mm could be identified, since amplitude differs a lot comparing to threaded area reflection amplitude.
Threaded are amplitude – 10.2 dB.
0,3 mm height notch amplitude – 6.4 dB

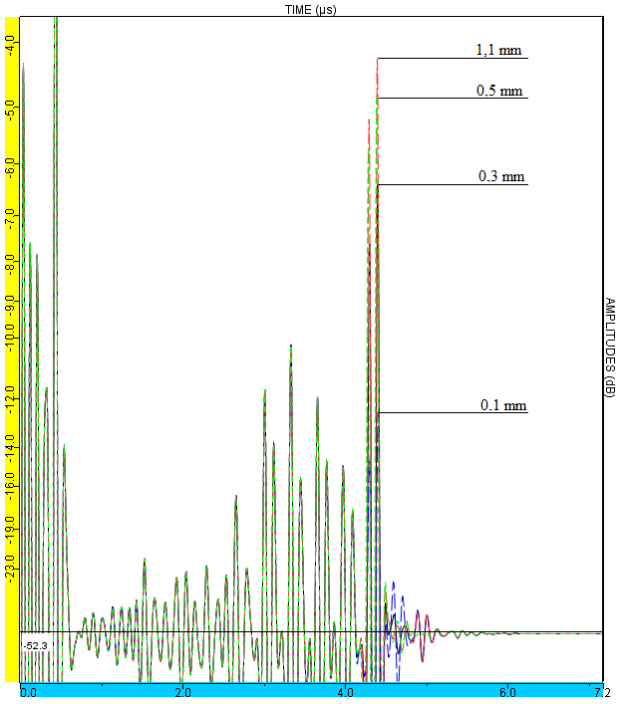

Figure 3-10. A-Scans of matrix phased array height variation

As per A-Scans obtained, in defect variation from 0,1 to 1,1 mm, increased amplitude and difference between 0,1 mm and 0,3 mm height defect could be noticed. In this area re-calculation of height variation is required to get more detailed results on how small defect could be identified with matrix phased array method.

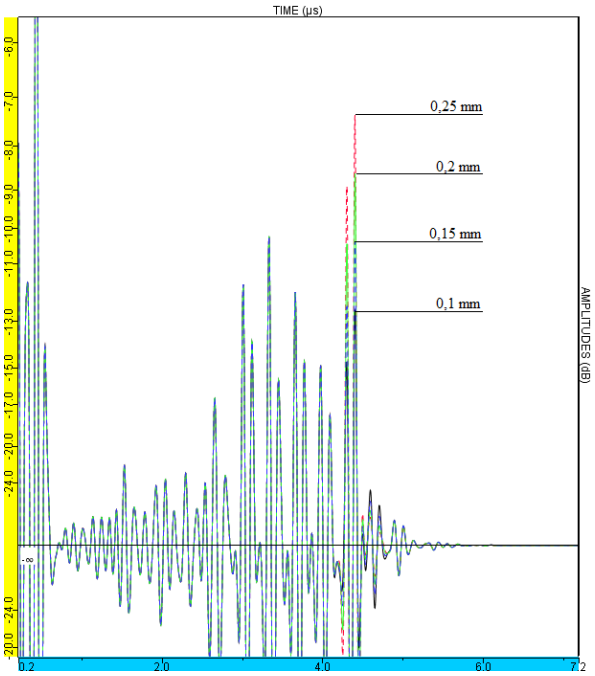

Figure 3-11. A-Scans of matrix phased array height variation of defects up to 0,25 mm height

As shown in figure 3.11. It could be noticed that smallest defect, which could be detected is 0,2 mm.
Threaded area amplitude – 10,2 dB.
Notch with 0,2 mm height amplitude – 8,6 dB.

3.7. Matrix phased array angle variation

During previous parametric calculations beam position and angle was fixed, however during angle variation calculation, beam angle will be adjusted without moving transducer elements to obtain more detailed results. The beam position configuration will remain 62.7 mm at Y-axis, radius will stay at 3.3 mm and angle will change according to variation angle. In total 10 variations will be performed from 0^0 to 90^0, each variation at 10^0 step.
For further comparison, A-Scans of 4 different angles as shown in figure 3.12 will be analyzed.

a) Notch located at 0^0.
b) Notch located at 30^0.
c) Notch located at 50^0.
d) Notch located at 90^0.

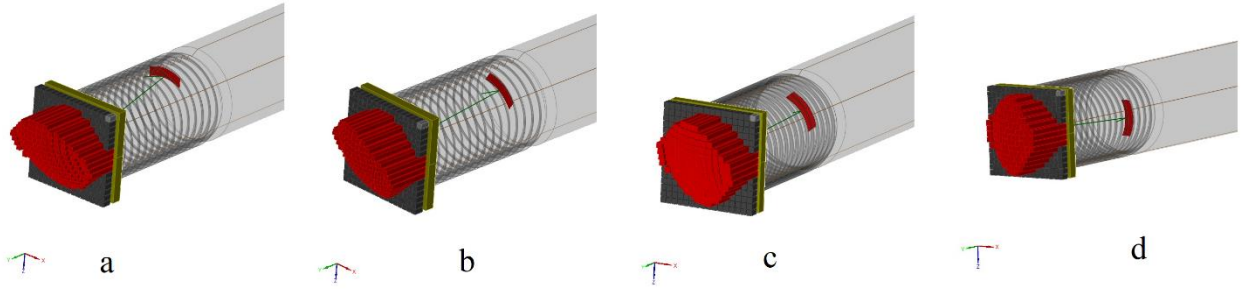

Figure 3-12. Angle variations during parametric studies

After parametric studies performed, A-Scans were obtained as shown in figure 3.13.

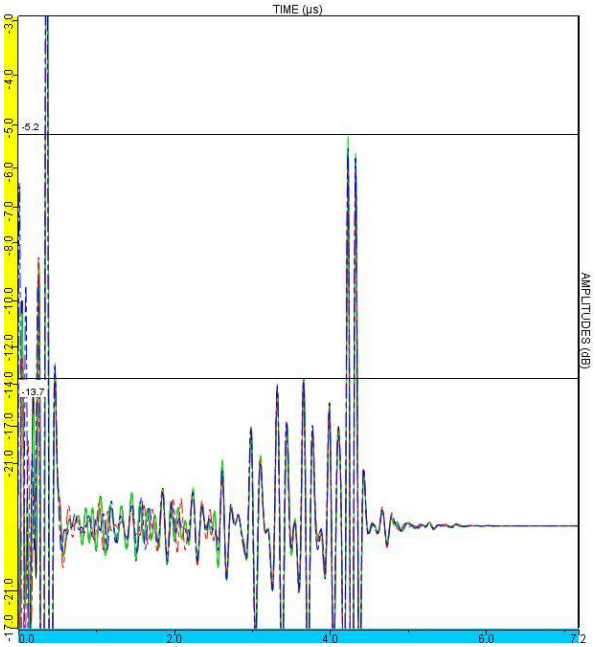

Figure 3-13. A-Scans of parametric studies on matrix phased array angle variation

It could be seen that with ability to move beam without moving the transducer elements, defects could be detected independent from angle. Independent from angle, defect amplitude is – 5,2 dB and reflection from threaded area has amplitude of -13,7 dB.

4. Contact immersion method comparison versus matrix phased array

For contact immersion and developed matrix phased array following calculations were performed.

1. During both methods, 3,8 mm height and 1 mm length defect was positioned on most critical areas: first incomplete thread root and third/forth complete thread root. A-Scans obtained, and amplitudes compared. During immersion method A-Scans were obtained, when probe was positioned in center area and on top of the bolt. During matrix phased array method, transducer elements was fixed to center position only.
2. Beam computation to find focal zone performed.
3. Parametric studies performed, while height, position and angle of notch were variated.

4.1. Initial flaw detect comparison

To configure both methods properly, exact same notches were designed and initially positioned to 1st and 3 or 4th thread root area. Initial calculations allow to see the difference in amplitudes and to understand where and how big is the defect. As shown in figure 4.1 combined A-Scans of ultrasound immersion and matrix phased array were obtained. It could be noticed that:

1. Matrix phased array has same notches amplitude of – 5.5 dB and much better visibility on the scan comparing to ultrasound immersion method. Both defects on both methods could be interpreted, however during ultrasound immersion method, defect amplitudes in A-Scan were similar to threaded area amplitude. Defect on forth complete thread root area - -22.8 dB, defect on first incomplete thread root area – 28.4 dB and threaded area -23.2 dB.
2. After initial calculation of ultrasound immersion method, it was decided to calculate focal zone to understand, which area on specimen has highest accuracy.

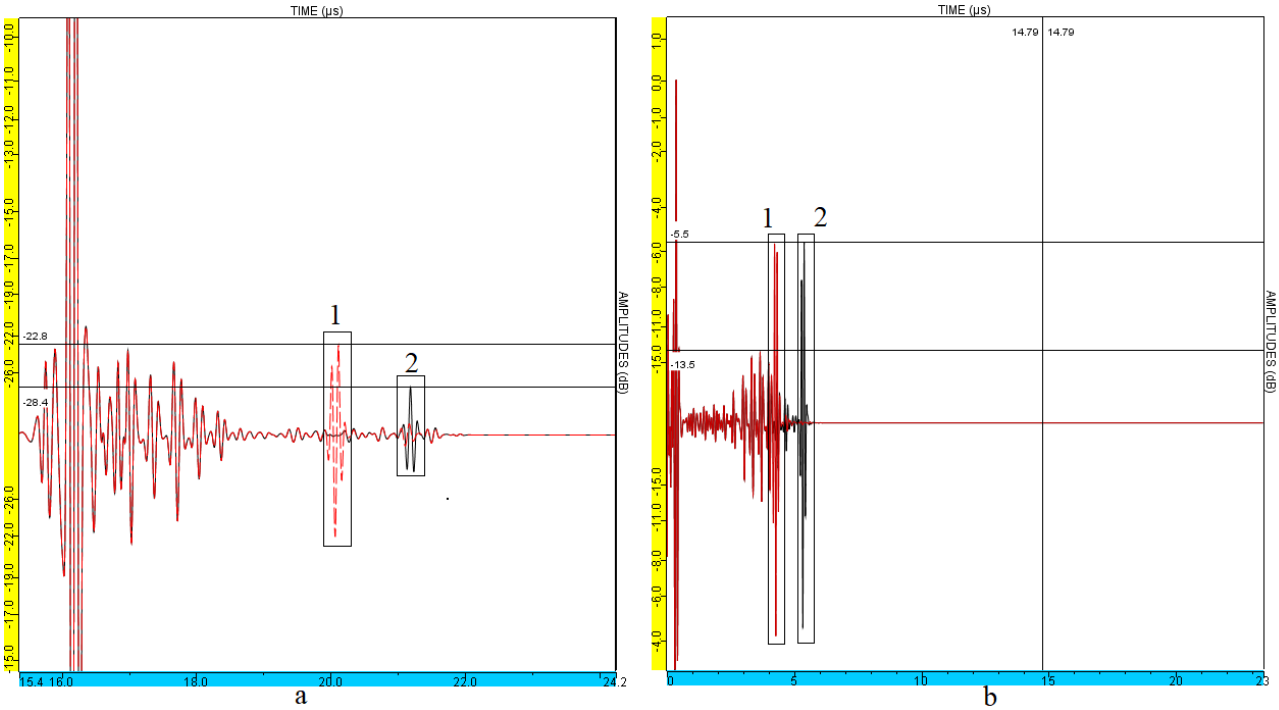

Figure 4-1. A-Scan of a) ultrasound immersion method and b) matrix phased array. 1 – notch at forth complete thread root area, 2 – notch at first incomplete thread root area

4.2. Beam computation comparison

During both methods beam focal zone computation were performed, while transducer position was fixed to specimen center position. As shown in figure 4.2.

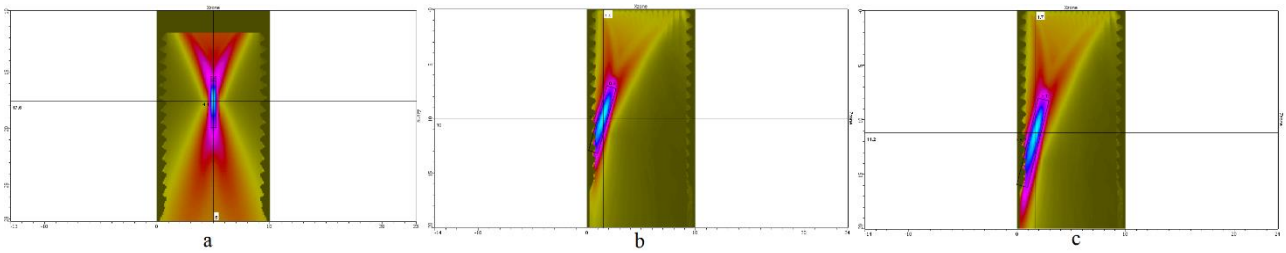

Figure 4-2. Beam focal zone computation. a) Ultrasound immersion method, b) matrix phased array beam focused at 3 and 4 complete thread area, c) matrix phased array beam focused at first incomplete thread root area

From results obtained it could be noticed that focal zone is concentrated in the centre of the tie-bolt, and is located between 7^{th} and 11^{th} thread area . Configured immersion method calculated focal zone is 0.5 mm width and 4.2 mm length, however this area would cover approximately 7-11^{th} thread area. As for matrix phased array, two computations performed, since this method provides an option to reposition focal zone, without moving transducer elements. On figure 4.2 b, focal spot configured to third/forth complete thread root area and focal zone dimensions were calculated. Focal zone found to be 0.9 mm width and 6.2 mm length. Increased focal zone allows to obtain more detailed A-Scan results. To evaluate how focal zone dimensions variates, repositioning of focal point to first incomplete thread root area were performed and calculations of focal zone completed. Focal zone calculated is 1 mm width and 8.2 mm length. Matrix phased array method computation proved that it has much higher accuracy area against ultrasound immersion method. Opportunity to change focal zone and move it in 2 dimensions decrease human error in interpreting the defects from A-Scan since amplitudes should have better dB ratio against ultrasound immersion method.

4.3. Parametric studies comparison

During parametric studies comparison it should be noted, that while using ultrasound immersion method, 2 probe positions were used. Matrix phased array method transducer elements fixed at one position.

4.4. Defect position variation comparison

Defect position variation computation has proved, that ultrasound immersion method could not detect any defects if probe position is incorrect. As per figure 4.3 when probe was positioned at specimen center area, we were not able to identify any defect amplitudes in combined A-Scans. Amplitude for all areas is identical. The reason of this is focal zone, which as calculated is not covering threaded areas if probe position is improper. This means that immersion method could lead to false identification of defect, while positioning the probe. Probe angle, water path and position on specimen could.

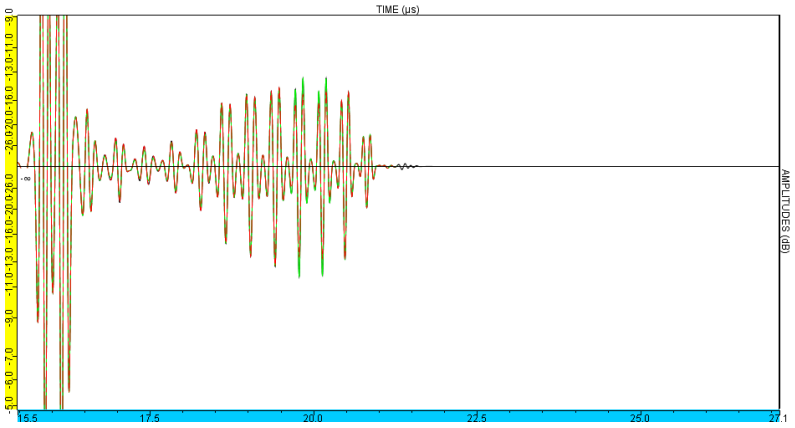

Figure 4-3. A-Scan of defects position variation using ultrasound immersion method

After probe position was changed to be in parallel with threaded area and defects, it was possible to receive A-Scans with defect amplitudes as shown in figure 4.4. Amplitudes with matrix phased array A-Scan and amplitudes with immersion method could be compared. Both graphs identifies defect as following:

1. Last threaded area
2. Forth complete thread root area
3. First incomplete thread root area

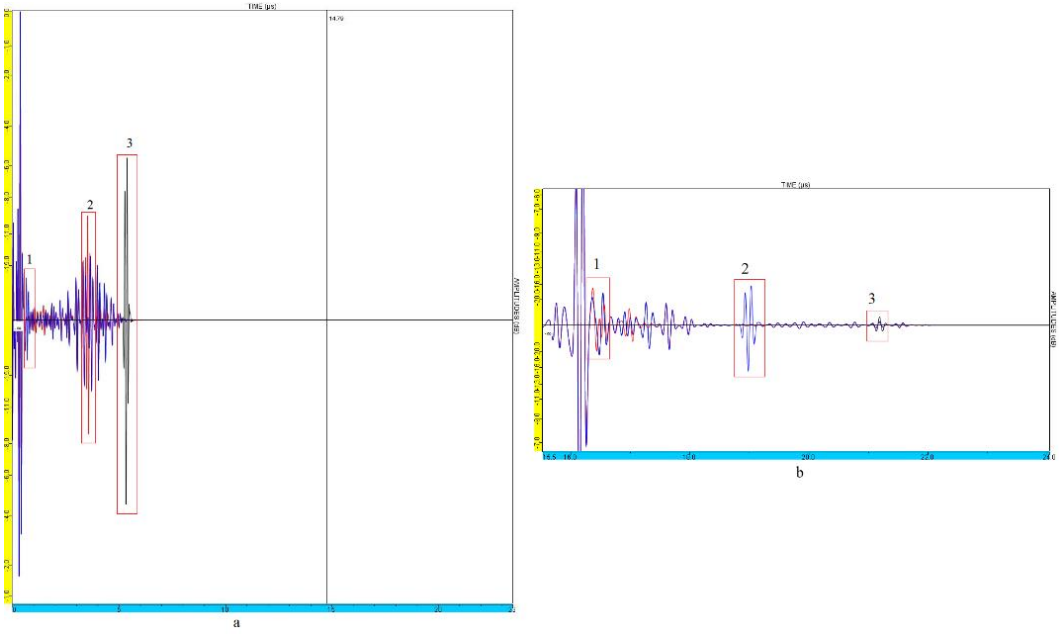

Figure 4-4. A-Scans of defect flaw variation

Matrix phased array method as shown in figure 4.4(a), provided much clearer A-Scans, since the defects amplitudes was higher than threaded area reflection, all 3 defects would be noticeable during inspection, however during ultrasound immersion method as shown in figure 4.4(b), only 1 defect was clearly visible and had higher amplitude then threaded area reflection. Forth complete thread root

area was located at ultrasound immersion beam focal zone. Matrix phased array ability to move focal zone, allows to see all three defects in combined A-Scans.

4.5. Defect flaw variation comparison

As calculated previously, when probe position is centered and using ultrasound immersion method, flaw variation A-Scan did not record any placed defects as shown in figure 4.5. As discussed previously, the reason for this is focal zone area, which does not cover placed defects.

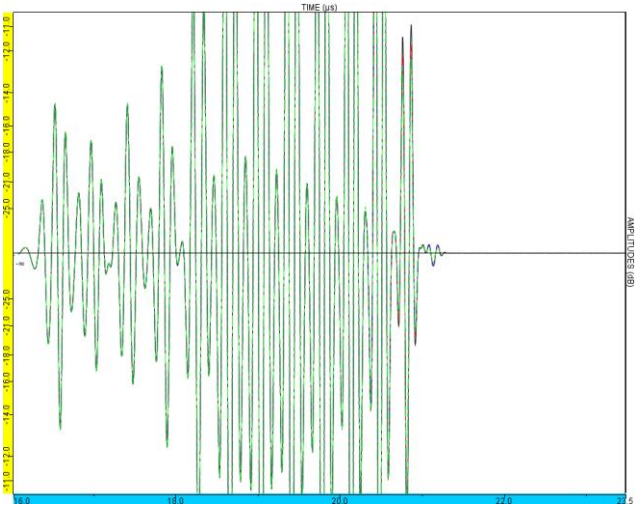

Figure 4-5. Ultrasound immersion method A-Scans of flaw variation

To see defects, probe position was moved parallel to threaded area and defects. In developed matrix phased array method, probe was fixed on center. As shown in figure 4.6 it could be noticed:

a) Ultrasound immersion method, probe positioned parallel to threaded area and defects.
b) Matrix phased array, transducer elements center position
c) Matrix phase array, detailed variation, up to 0,25 mm notch height.

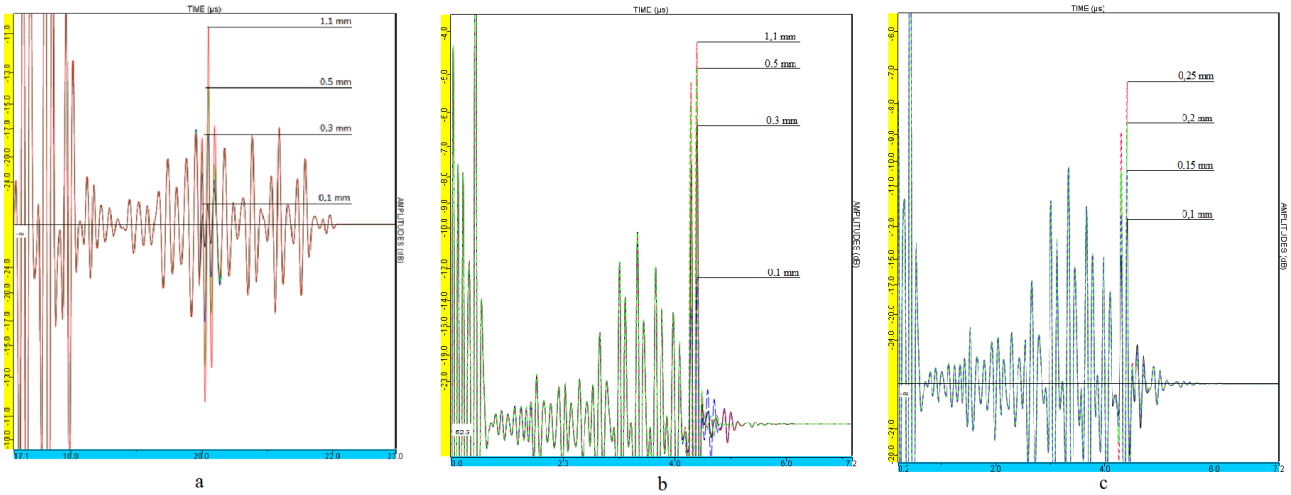

Figure 4-6. A-Scans of flaw variation, while using ultrasound immersion method (a), Matrix phased array method (b, c)

Results from A-Scans shown in figure 4.6 could conclude that matrix phased array could detect defects as small as 0,2 mm, while ultrasound immersion method is capable to detect defects starting from 0,4-0,5 mm. The main reason for this is ability to move matrix phased array beam focal point in 2 dimensions.

4.6. Defect angle variation comparison

When using ultrasound immersion method and probe positioned on specimen center, defects could not be found due to small focal zone. A-Scans obtained from parametric studies could be seen in figure 4.7.

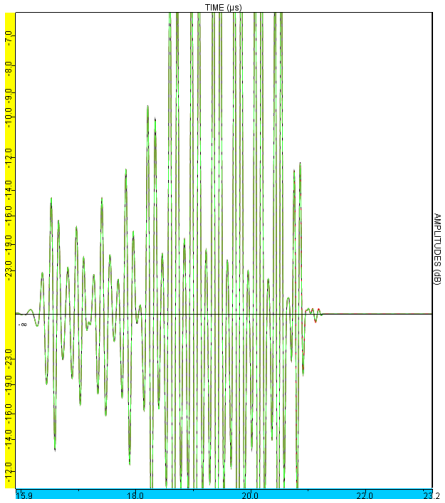

Figure 4-7. Ultrasound immersion A-Scans of defect angle variation

When probe was positioned parallel to the threads and defect located at 0^0, A-Scans were obtained and compared with matrix phased array scans as shown in figure 4.8.

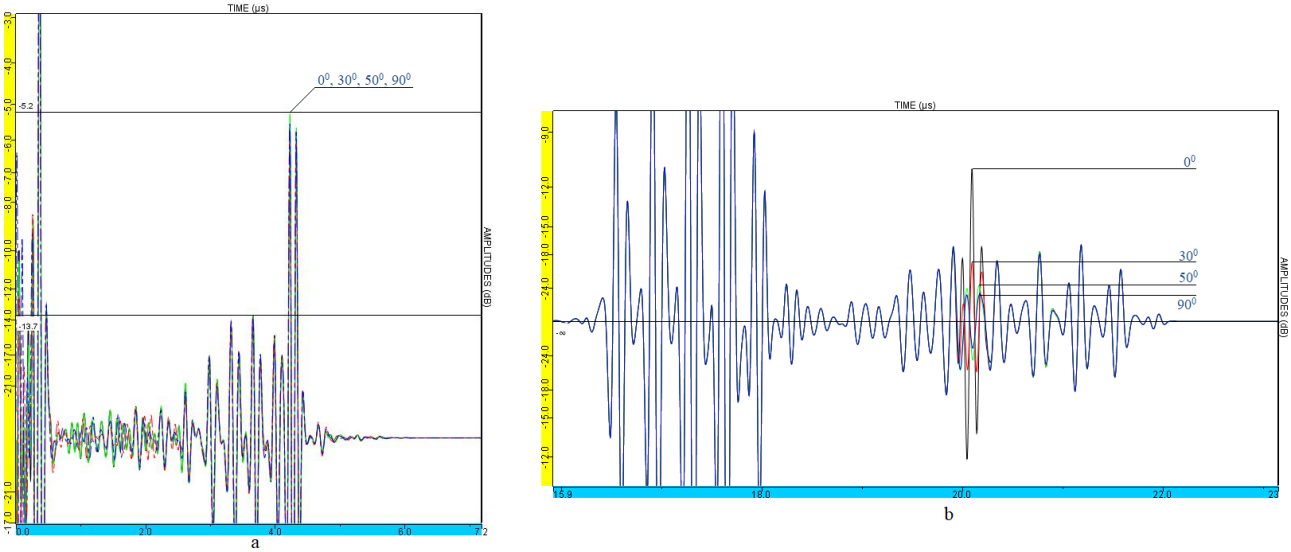

Figure 4-8. Matrix phased array A-Scans of defect angle variation (a), ultrasound immersion A-Scans of defect angle variation (b)

As shown in figure 4.8 ultrasound immersion method (b), only defect located at 0^0 could be detected in A-Scan, since it is located in focal zone. Matrix phased array (a) provides an option to change focal zone. Due to this option, defect could be detected independently from angle variation.

Conclusions

1. It was determined that currently used methods for tie-bolt crack inspection like eddy current, dye penetrant, magnetic particle inspection or ultrasound immersion pulse-echo method are effective not in all cases. Ultrasonic inspection method using phased array could allow to increase detectability rate, as it gives more possibilities like electronic scanning and steering of the beam.

2. Beam computation and parametric studies have been performed for currently used ultrasonic immersion pulse-echo method. It was determined, that while performing inspection with currently used method, focal zone is concentrated in the centre of the tie-bolt and is located between 7^{th} and 11^{th} thread area, while cracks usually form in the zone between first incomplete thread root to forth complete thread root areas. Therefore, it was determined, that currently used set-up is not optimal for the reliable detection of cracks in tie bolts.

3. Parametric studies of influence of height, position, and angle of defects on detectability were performed. It was determined, that currently used technique enables to find only defects in between focal zone located between 7^{th} and 11^{th} threaded area and bigger than 0,5 mm, located only in front of the transducer.

4. Ultrasonic inspection method while using matrix phased array was developed. It was determined, that using proposed method defects from 0,2 mm could be detected. Possibility of electronical scanning and steering allows to detect defects, which are located at any depth and position in the tie-bolt.

5. Matrix phased array method was compared to ultrasound immersion method. It was determined that matrix phased array method with 16x16 elements would be more suitable method for defects detection due to ability to perform electronical scanning and steering in 3D.

List of References

1. **HUGH, J**. Cause and effect diagrams. *Engineering Design, Planning, and Management.* 2013, pp. 323-325. ISBN 978-0-12-397158-6. Access via Science Direct

2. **ROHIT, B., P. D. Gowda, N. B. Nagaraju, and S. Meghana**. Life and Failure of Aircraft Wheels - A Review. *IOP Conference Series: Materials Science and Engineering*. 2019, vol. 520, no. 1. DOI: 10.1088/1757-899X/520/1/012002.

3. **ECCLES, B**. Fatigue Failure of Bolts, [Online]. Available: https://www.boltscience.com/pages/fatigue-failure-of-bolts.pdf

4. **YILMAZ, O., C. Jiménez-Peña, and D. Debruyne**. Fatigue response of high-strength steel bolted connections under in-plane shear and out-of-plane bending loading modes. *Procedia Structural Integrity*. 2019, vol. 19, pp. 302-311. DOI: 10.1016/j.prostr.2019.12.033.

5. *ATSB Transport Safety Report Aviation Occurrence Investigation Main landing gear wheel failure during taxi involving Boeing 737, VH-VUH*. [Online]. 2017. Available: www.atsb.gov.au.

6. **KOBAYASHI, T., and D. A. Shockey**. Analysis of failed aircraft wheel assembly. *Engineering Failure Analysis*. 2006, vol. 13, no. 1, pp. 65–74. DOI: 10.1016/j.engfailanal.2004.12.046.

7. **POON, K**. Fatigue Testing 101. *Quality Magazine*. 2019. Available: https://www.qualitymag.com/articles/95702-fatigue-testing-101

8. **WANG, J., B. Uy, D. Li, and Y. Song**. Fatigue behaviour of stainless steel bolts in tension and shear under constant-amplitude loading. *International Journal of Fatigue*. 2020, vol. 133. DOI: 10.1016/j.ijfatigue.2019.105401.

9. *ATR 42-500 Aircraft Maintenance Program*. Issue 1, rev 13. 2021.

10. *ATR 42-300 Aircraft Maintenance Manual*. Rev 13, Nov 2019.

11. **GRECO, A., A. de Luca, G. Lamanna, and R. Sepe**. Numerical investigation on the influence of tightening in bolted joints. *Procedia Structural Integrity*. 2019, vol. 24, pp. 746–757. DOI: 10.1016/j.prostr.2020.02.066.

12. **DEN OTTER, C., and J. Maljaars**. Preload loss of stainless steel bolts in aluminium plated slip resistant connections. *Thin-Walled Structures.* 2020, vol. 157. DOI: 10.1016/j.tws.2020.106984.

13. *Flight Data Monitoring On ATR Aircraft*. 2016.

14. **OEHLING, J., and D. J. Barry**. Using machine learning methods in airline flight data monitoring to generate new operational safety knowledge from existing data. *Safety Science*. 2019, vol. 114, pp. 89–104. DOI: 10.1016/j.ssci.2018.12.018.

15. **DU, W., Y. Zhao, R. Roy, S. Addepalli, and L. Tinsley**. A review of miniaturized Non-Destructive Testing technologies for in-situ inspections. *Procedia Manufacturing.* 2018, vol. 16, pp. 16–23. DOI: 10.1016/j.promfg.2018.10.152.

16. **GRANDT, F., Jr**. Damage tolerant design and non-destructive inspection - Keys to aircraft airworthiness. *Procedia Engineering.* 2011, vol. 17, pp. 236–246. DOI: 10.1016/j.proeng.2011.10.025.

17. **GHOLIZADEH, S**. A review of non-destructive testing methods of composite materials. *Procedia Structural Integrity*. 2016, vol. 1, pp. 50–57. DOI: 10.1016/j.prostr.2016.02.008.

18. **ENDRAMAWAN, T., and A. Sifa**. Non Destructive Test Dye Penetrant and Ultrasonic on Welding SMAW Butt Joint with Acceptance Criteria ASME Standard. *IOP Conference Series: Materials Science and Engineering*. 2018, vol. 306, no. 1. DOI: 10.1088/1757-899X/306/1/012122.

19. *NDT Manual Penetrant Inspection*. 2005.

20. **LI, L., Y. Yang, X. Cai, and Y. Kang**. Investigation on the formation mechanism of crack indications and the influences of related parameters in magnetic particle inspection. *Applied Sciences (Switzerland)*. 2020, vol. 10, no. 19. DOI: 10.3390/app10196805.

21. **ZOLFAGHARI, A., A. Zolfaghari, and F. Kolahan**. Reliability and sensitivity of magnetic particle non-destructive testing in detecting the surface cracks of welded component. *Non-destructive Testing and Evaluation.* 2018, vol. 33, no. 3, pp. 290–300. DOI: 10.1080/10589759.2018.1428322.

22. *AP-763 Nondestructive Testing Manual*. 2005.

23. **KONG, Y., C. J. Bennett, and C. J. Hyde**. A review of non-destructive testing techniques for the in-situ investigation of fretting fatigue cracks. *Materials and Design*. 2020, vol. 196. Elsevier Ltd. DOI: 10.1016/j.matdes.2020.109093.

24. **JANOVEC, M., M. Smetana, and M. Bugaj**. Eddy current array inspection of Zlin 142 fuselage riveted joints. *Transportation Research Procedia.* 2019, vol. 40, pp. 279–286. DOI: 10.1016/j.trpro.2019.07.042.

25. **SUN, H., T. Wang, D. Lin, Y. Wang, and X. Qing**. An eddy current-based structural health monitoring technique for tracking bolt cracking. *Sensors (Switzerland)*. 2020, vol. 20, no. 23, pp. 1–14. DOI: 10.3390/s20236843.

26. **SCHNARS, U., and R. Henrich**. Applications of NDT Methods on Composite Structures in Aerospace Industry.

27. **JASIŪNIENĖ, E., E. Žukauskas, V. Samaitis, R. Rekuvienė**. Non-Destructive Testing. 2019. ISBN 978-609-02-1647-7.

28. **HILL, S., and S. Dixon**. Localization of defects with time and frequency measurements using pulsed arrays. *NDT and E International*. 2014, vol. 67, pp. 24–30. DOI: 10.1016/j.ndteint.2014.06.008.

29. **LIAPTSIS, G., P. Charlton, D. Liaptsis, and B. Wright**. Focal Law Calculations for Annular Phased Array Transducers. 2015. [Online]. ISSN: 1435-4934.

30. **POGUET, J**. Phased Array technology: concepts, probes and applications. 2002, vol. 7, no. 05. Available: https://www.ndt.net/article/v07n05/poguet/poguet.htm

31. **CHO, S., H. Jeong, and I. K. Park**. Optimal design of annular phased array transducers for material nonlinearity determination in pulse–echo ultrasonic testing. *Materials.* 2020, vol. 13, no. 23, pp. 1–19. DOI: 10.3390/ma13235565.

32. **MOLES, M., and R. Ginzel**. Phased Arrays for Detecting Cracking in Bolts. *Other MajorComponent Inspection II*. [Online]. 2007. Available: www.ndt.net/search/docs.php3?MainSource=70.

33. *What CIVA brings to NDT*. [Online]. Available: www.extende.com.

34. *Ultrasonic testing with CIVA*. [Online]. Available: www.extende.com.

35. *The Simulation & Analysis Platform for NDT*. [Online]. Available: www.extende.com

36. *MS21250 Bolt, Tension, Steel, External Wrenching, Flanged, 12-Point, 180KSI Ftu, 450°F*. [Online]. Available: www.abbottaerospace.com

37. **S.Mahaut, S.Loone, L.Roumilly.** *Validation of CIVA Simulation Tools for Ultrasonic Inspection in Realistic Configuration.* 2006.[Online]. ESNDT 2006 – We.1.4.4.

38. *Beam characterization of immersion probe on solid inclusions and an infinite plane.* [Online]. Available: www.extende.com.

39. **G. Holmer, W. Daniels, T. Zettervall.** *Evaluation of the simulation software CIVA for qualification purpose. 2017.* [Online]. ISSN: 2000-0456

40. **REVERDY, F., L. le Ber Eddyfi, S. Mahaut, P. Dubois, L. le Ber, and O. Roy**. Advanced Matrix Phased Array Settings for Inspection. 2008. [Online]. Available: https://www.researchgate.net/publication/229035105.